Journal of Advances in Mathematics and Computer Science

28(5): 1-30, 2018; Article no.JAMCS.43101
ISSN: 2456-9968
(Past name: British Journal of Mathematics & Computer Science, Past ISSN: 2231-0851)

Numerical Investigation of Natural Convection Flow in a Trapezoidal Cavity with Non-uniformly Heated Triangular Block Embedded Inside

Muhammad Sajjad Hossain[1,2*], Md. Abdul Alim[3] and Laek Sazzad Andallah[2]

[1]Department of Arts and Sciences, Ahsanullah University of Science and Technology, Dhaka-1208, Bangladesh.
[2]Department of Mathematics, Jahangirnagar University, Dhaka-1342, Bangladesh.
[3]Department of Mathematics, Bangladesh University of Engineering and Technology, Dhaka-1000, Bangladesh.

Authors' contributions

This work was carried out in collaboration between all authors. Author MSH designed the physical model, wrote the literature review, carried out simulation work, wrote the first draft of the manuscript and did the analysis of the study. Author MAA provided the idea of the problem, helped to match the program, checked the overall write up, figures, numerical results and data. Author LSA discussed the idea of the problem, checked the numerical results and the whole manuscript. All authors read and approved the final manuscript.

Article Information

DOI: 10.9734/JAMCS/2018/43101
Editor(s):
(1) Dr. Francisco Welington de Sousa Lima, Professor, Dietrich Stauffer Laboratory for Computational Physics, Departamento de Física, Universidade Federal do Piaui, Teresina, Brazil.
Reviewers:
(1) Fateh Mebarek Oudina, University of Skikda, Algeria.
(2) Prasun Dutta, Indian Institute of Engineering Science and Technology, Shibpur, India.
(3) A. M. Kawala, Helwan University, Egypt.
Complete Peer review History: http://www.sciencedomain.org/review-history/26101

Original Research Article

Received: 12 June 2018
Accepted: 18 August 2018
Published: 04 September 2018

Abstract

The present numerical attempt deals with the analysis of natural convection flow in a trapezoidal cavity with triangular block embedded inside intended for various inclination angles ϕ. In this cavity, the bottom wall is non-uniformly heated, left and right (side) walls are cold and the top wall is well insulated. The triangular block or triangular solid body surface for different positions (LBC, RBC, LTC, RTC) inside the trapezoidal cavity is also non-uniformly heated (T_{hb}). A Galerkin weighted residual finite element method is applied to solve the Navier-Stokes equations and energy balance equations and to find the results in the form of streamlines, isotherms (temperature), heat function, pressure and local Nusselt numbers and average Nusselt number for different parameters. Finite element method has also been used to solve the

**Corresponding author: E-mail: msh80_edu@yahoo.com;*

velocity and thermal fields. The fluid is concerned for various governing parameters, such as Rayleigh number, Ra ($10^3 \leq Ra \leq 10^6$), Prandtl number, Pr ($0.026 \leq Pr \leq 1000$) and various inclination angles ϕ (ϕ = 45°, 30° and 0°). It has been revealed that due to non-uniformly heated triangular block, heatlines by connecting cold and hot walls are found to be continuous lines and also perpendicular to the isothermal walls which occur for the conduction dominant regimes. Fluid flow and heat flow occur symmetrically. The local Nusselt number and average Nusselt number for the non-uniformly heated bottom wall of the trapezoidal cavity using the inside of the non-uniformly heated triangular block are illustrated by heatlines. It has been also found that heat transfer rates significantly depend on the tilt angles (ϕ), non-uniformly heated triangular block and aforementioned non-dimensional parameters.

Keywords: Natural convection; Galerkin weighted residual finite element method; trapezoidal cavity; triangular block; non-uniform heating.

NOMENCLATURES

g	*Acceleration due to gravity(m/ s^2)*
Gr	*Grashof number*
H	*Convective heat transfer coefficient (W/m^2 K)*
k	*Thermal conductivity of fluid(W/m K)*
L	*Height or base of trapezoidal cavity (m)*
N	*Total number of nodes*
Nu_{av}	*Average Nusselt number*
Nu_{local}	*Local Nusselt number*
P	*Non-dimensional pressure*
p	*Pressure, Pa*
Pr	*Prandtl number*
Ra	*Rayleigh number*
T	*Temperature (K)*
T_h	*Temperature of hot bottom wall (K)*
T_c	*Temperature of cold side wall (K)*
U	*x component of non-dimensional velocity*
u	*x component of velocity (m/s)*
V	*y component of non-dimensional velocity*
v	*y component of velocity (m/s)*
V_0	*Lid velocity*
x, y	*Distance along Cartesian coordinates*
X,Y	*Dimensionless distance along Cartesian coordinates*
T_i	*Temperature of insulated top wall (K)*
LBC	*Left bottom configuration*
RBC	*Right bottom configuration*
LTC	*Left top configuration*
RTC	*Right top configuration*
T_{hb}	*Non-uniformly heated wall of triangular block*

GREEK SYMBOLS

α	*Thermal diffusivity (m^2/s)*
β	*Coefficient of thermal expansion (K^{-1})*
ρ	*Density of the fluid (kg/m^3)*
$\Delta\theta$	*Temperature difference*
μ	*Dynamic viscosity of the fluid (Pa s)*
ν	*Kinematic viscosity of the fluid (m^2/s)*
ψ	*Stream function*
θ	*Dimensionless temperature*
Π	*Heatfunction*
σ	*Fluid electrical conductivity($\Omega^{-1}m^{-1}$)*
ϕ	*Inclination angles*

SUBSCRIPTS

b	*Bottom wall*
l	*Left wall*
r	*Right wall*
s	*Side wall*

1 Introduction

Natural convection, fluid flow and heat transfer in enclosed cavities especially inside an enclosure has long been studied and has attracted many researchers due to large number of engineering applications, such as, nuclear reactors, design of solar collectors, thermal design of buildings, lakes and reservoirs, air conditioning, cooling of electronic devices, food processing, crystal growth and solidification process applications etc. [1-6]. Studies of natural convection are carried out for different square, rectangular, triangular and trapezoidal cavities. In recent years, a considerable attention has been received by trapezoidal cavities for its application in various fields. As one of the representative geometries, laminar natural convection with triangular body surface inside a trapezoidal cavity is of great interest, since such type of geometry is applied as engineering applications which have been discussed above. A brief account of relevant literature on convection patterns in cavities is presented below.

The penalty finite element analysis with bi-quadratic elements was studied by Basak et al. [7] to find out the weight of uniform and non-uniform heating of base wall within a trapezoidal field of various leaning angles φ taking an ample range of Rayleigh number ($10^3 \leq Ra \leq 10^6$), Prandtl number 0:026 ≤ Pr ≤ 6 988:24) and Darcy number, ($10^3 \leq Da \leq 10^5$). It is pragmatic that the adjacent heat transport rate at the middle portion of the base wall is bigger for non-uniform heating crate and also observed that the average warm transfer rate at the base wall is established to be invariant regarding φ at higher Ra in favour of non-uniform heating. An inclusive heatline appears for natural convection streams in trapezoidal enclosures with the result of diverse walls heating [8]. Besides, the occurrence of natural convection with a porous matrix in a trapezoidal enclosure has been discussed mathematically by Basak et al. [9]. Numerical research of natural convection for uniformly or non-uniformly heated underneath wall in porous trapezoidal enclosures was conducted by Basak et al. [10] using penalty finite element analysis with bi-quadratic elements to find out the Navier–Stokes and energy balance equations. It has been initiated that secondary circulations come out at the top angles of the hollow for $\varphi = 45^{\circ}$, 60° and bottom corners of the cavity for $\varphi = 90^{\circ}$ with Pr = 0.015, $Da = 10^{-3}$ and $Ra = 10^6$. It is found that Nu_b values are greatest near the corners of bottom wall for all φ's irrespective to Da and Pr due to the heated underneath wall with freezing side walls. Local Nusselt number (Nu_b) is least near the corners of the underneath wall and is also seen a sinusoidal variation with distance for all angles φ at high Da. Khozeymehnezhad and Mirbozorgi [11] carried out the numerical computations for natural convection among a freezing outer square enclosure and a hot interior cylinder stimulated by a temperature difference for two different geometries. The results explained that when an inner cylinder is placed at a certain distance from the middle of the enclosure then the division from the bicellular vortices to a uni-cellular vortex occurs for both cylinders, and also at small Rayleigh numbers. It has been also found that the heat transfer rate from the enclosure is superior than the inside position of the circular cylinder. Study of thermal management via distributions of heatlines and entropy generation for natural convection in trapezoidal cavities was studied by Ramakrishna et al. [12] for the variety of parameters, such as Darcy numbers, Prandtl numbers, Rayleigh numbers based on heatline concept. In this work, the thermal mixing is magnified as Da enhances from 10^{-5} to 10^{-3}. Besides, the thermal gradients are very close to the lower part of the left wall and upper part of the right wall for $Da \geq 10^{-4}$ irrespective of φ and Pr and also, the thickness of the thermal frontier layer is small beside those areas. It has been also analysed that at higher Da, total entropy generation is high for Pr = 1000 than Pr = 0.015. Moreover, heat stream patterns with heatline concept in the company of natural convection within trapezoidal enclosures taking uniformly and non-uniformly heated bottom wall, insulated top wall and isothermal side walls with inclination angles φ were investigated by Basak et al. [13]. The local Nusselt numbers show the results for side and underneath walls and variation of local Nusselt numbers with distance have also been explained based on heatlines. Furthermore, the significant variation of average heat transfer with φ is not seen for non-uniform heating of underneath wall. Hossain and Alim [14,15] also examined numerical simulation of magneto-hydrodynamic free convection within the trapezoidal cavity with the help of uniformly and non-uniformly heating of the bottom wall, insulated top wall and isothermal side walls for variety of parameters, such as Rayleigh number (Ra) from 10^3 to 10^7 and Prandtl number (Pr) from 0.026, 0.7, 1000 with liking angles $\varphi = 45°$, 30° and 0°. Heat flow patterns via heatline concept have been analysed within this trapezoidal enclosure. Besides, finite element computational simulations were carried out by Aparna and Seetharamu [16] for natural convection filled by porous media in a trapezoidal cavity to investigate the effect of uniformly and non-uniformly heated bottom wall. This study observes that the uniform temperature at the underneath wall of the enclosure gives a higher Nusselt number as compared to the linear and sinusoidally varying temperature cases and average Nusselt numbers raises because of raising Rayleigh number for underneath wall and the top wall. Alsabery et al. [17] studied the complexity of natural convection partially filled with nanofluid porous layer and partly with non-Newtonian fluid layer within a trapezoidal cavity and shown that convection increases via the addition of silver–water nanofluid and the heat transfer rate is affected with the inclination angle of the cavity variation. Laminar steady state natural convection in a two-dimensional even trapezoidal enclosure with a finite element method was studied by Uddin and Saha [18]. From this research, it is found that the average Nusselt number increases with the increase of Rayleigh number and due to higher Rayleigh number, the effect of the sidewall inclination angle on heat transfer is significantly reduced means decreases with the increase of base wall tilt. Fateh Mebarek-oudina and Rachid Bessaïh [19] studied a cylindrical configuration filled with a low-Prandtl number electrically conducting fluid convection, under the influence of either axial or radial magnetic field using finite volume method. In this investigation,

stability diagrams of liquid metal flow in natural convection have been confirmed by a radial magnetic field. A numerical research among vertical coaxial cylinders and under the influence of oscillatory magneto hydrodynamic natural convection of liquid metal was carried out by F. Mebarek-Oudina and R. Bessaih [20]. In this study, the flow stability and heat transfer rate have been controlled in varying the aspect ratio, intensity and route of the magnetic field. The stability of natural convection heat transfer in a cylindrical annular taking discrete isoflux heat source of different lengths has been investigated by F. Mebarek-Oudina [21]. The results indicate that the critical Rayleigh number decreases due to increase of heat source length ratio and flow stability and heat transfer rate can be controlled in varying of the heat source. The onset of oscillatory swirling liquid metal flow in a cylindrical container subjected to a vertical temperature gradient and an axial magnetic field has been studied by F. Mebarek-Oudina and Rachid Bessaïh [22]. The effect of the conductivity on the flow of the bottom wall and the rotating disk was shown in this research. Stability on the flow of natural convection in a cylindrical enclosure due to the magnetic field in Czochralski Crystal Growth is performed by F. Mebarek-Oudina and Rachid Bessaïh [23]. It is seen that owing to the increase of the magnetic field parameter, stability diagrams strongly depend on the critical Rayleigh number.

Motivated via the above mentioned investigations, it is pointed out that a little work has been done on natural convection flow in a trapezoidal cavity but, there is no noteworthy information for natural convection flow where a non-uniformly heated triangular block for different positions (LBC, RBC, LTC, RTC) exists in a trapezoidal cavity for assorted angles ϕ. The effect of the geometry of the heat transfer characteristics is necessary to learn to attain the optimal design of the container for a variety of industrial applications. The aim of the present article is to provide a complete presentation about the problem, solution procedure and detailed inspection which addresses the effects of heat flow via heatlines for natural convection within a trapezoidal cavity with the non-uniformly heated triangular block for different governing parameters Ra and Pr varying the diverse inclination angles ($\phi = 45^{\circ}, 30^{\circ}$ and 0°). Numerical results are obtained here in terms of the isotherms, heat function or total heat flux, pressure contours, and flow fields on heat transfer, heat transfer rate as well as the local Nusselt number and average Nusselt number of the fluid in the cavity for various materials with the ample range of Ra and Pr.

2 Physical Configuration

The schematic view of the problem of a two dimensional trapezoidal cavity of height L with the left wall inclined at an angle ϕ = 45°, 30°, 0° with Y- axis embedded inside a non-uniformly heated triangular block (T_{hb}) for various positions (LBC, RBC, LTC, RTC) are premeditated and illustrated in Fig. 1.0a-c (LBC). A Cartesian coordinate system is used with origin at the left corner of the computational domain. In a two-dimensional trapezoidal cavity, the bottom wall is considered with a non-uniform hot temperature (T_h) while the left and right (i.e. side) walls are considered at a cold temperature (T_c) and the top wall is kept thermal insulated (T_i). Here $T_h > T_c$. All the fluid properties are presumed to be constant and the boundary conditions for velocity are measured as no-slip on solid boundaries.

3 Mathematical Principal Equations

In the present problem, the two dimensional trapezoidal cavity is filled with an incompressible, Newtonian fluid and the flow is assumed to be steady, laminar and obeying Boussinesq approximation and there is no viscous dissipation. The steady dominant equations of conservation of mass, momentum and energy in the non-dimensional form Basak et al. [13] are offered as follows:

$$\frac{\partial U}{\partial X}+\frac{\partial V}{\partial Y}=0 \tag{1}$$

$$U\frac{\partial U}{\partial X}+V\frac{\partial U}{\partial Y}=-\frac{\partial P}{\partial X}+\Pr\left(\frac{\partial^2 U}{\partial X^2}+\frac{\partial^2 U}{\partial Y^2}\right) \tag{2}$$

$$U\frac{\partial V}{\partial X}+V\frac{\partial V}{\partial Y}=-\frac{\partial P}{\partial Y}+\Pr\left(\frac{\partial^2 V}{\partial X^2}+\frac{\partial^2 V}{\partial Y^2}\right)+Ra\,\Pr\,\theta \tag{3}$$

$$U\frac{\partial \theta}{\partial X}+V\frac{\partial \theta}{\partial Y}=\left(\frac{\partial^2 \theta}{\partial X^2}+\frac{\partial^2 \theta}{\partial Y^2}\right) \tag{4}$$

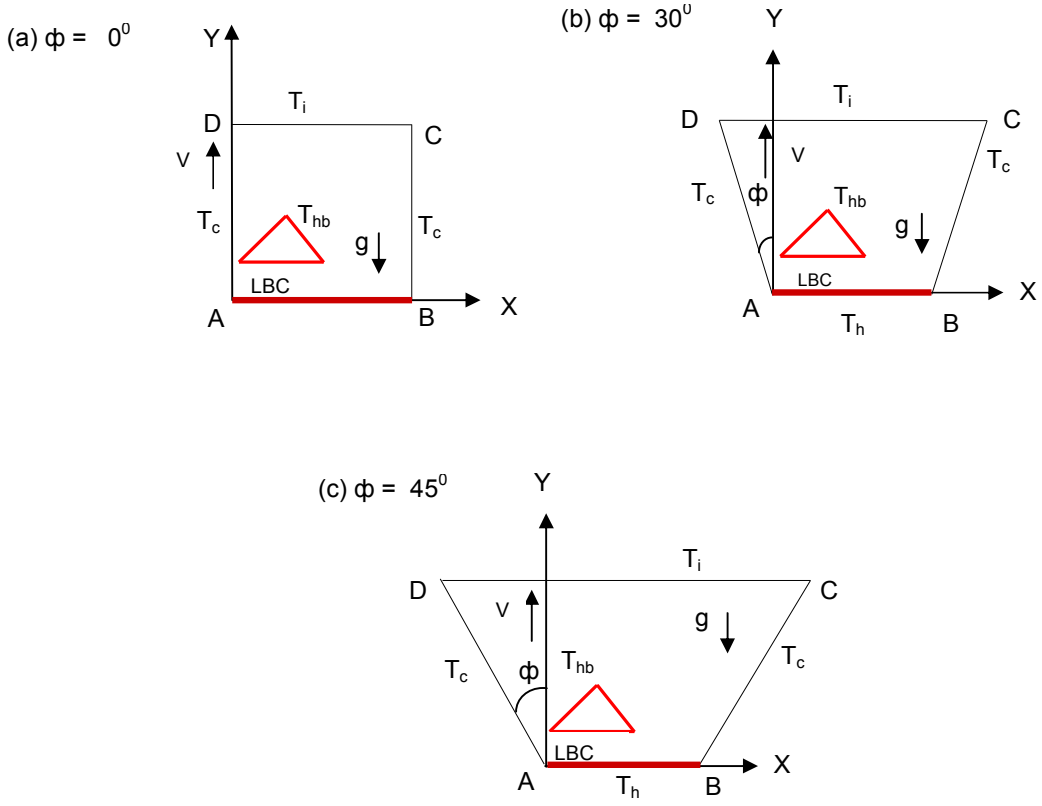

Fig. 1. Schematic diagram of the physical system for (a) ϕ = 0° , (b) ϕ = 30° and (c) ϕ = 45°

The above equations (1) - (4) are non-dimensionalised with the following dimensionless variables [13]:

$$X=\frac{x}{L},\quad Y=\frac{y}{L},\quad U=\frac{uL}{\alpha},\quad V=\frac{vL}{\alpha},\quad \Pr=\frac{\nu}{\alpha},\quad \theta=\frac{T-T_c}{T_h-T_c},$$

$$P=\frac{pL^2}{\rho\alpha^2},\quad Gr=\frac{g\beta L^3\left(T_h-T_c\right)}{\nu^2},\quad Ra=\frac{g\beta L^3\left(T_h-T_c\right)\Pr}{\nu^2}$$

and the corresponding boundary conditions Basak et al. [13] (Fig. 1), for the current problem are specified as follows:

At the bottom wall: $U=0,\quad V=0,\quad \theta=\sin\left(\pi X\right)\quad \forall\, Y=0,\quad 0\le X\le 1$

At the left wall: $U=0,\quad V=0,\quad \theta=0,\quad \forall\, X\cos\phi+Y\sin\phi=0,\quad 0\le Y\le 1$

At the right wall: $U=0,\quad V=0,\quad \theta=0,\qquad \forall\ X\cos\phi - Y\sin\phi=\cos\phi,\quad 0\le Y\le 1$

At the top wall: $U=0,\quad V=0,\quad \dfrac{\partial\theta}{\partial Y}=0,\qquad \forall\ Y=1,\quad -\tan\phi\le X\le(1+\tan\phi)$

At the different positions (LBC, RBC, LTC, RTC) of triangular block surface:

$$U(X,Y)=0,\quad V(X,Y)=0,\quad \theta(X,Y)=\sin(\pi X)$$

Where X and Y are dimensionless coordinates varying along horizontal and vertical directions, respectively; U and V are the dimensionless velocity components in X and Y directions, respectively; θ and P are the dimensionless temperature and pressure and *Ra, Pr, Gr* are Rayleigh number, Prandtl number and Grashof number, respectively. Thermal diffusivity, volumetric thermal expansion coefficient, kinematic viscosity, density and the dimensional temperature difference of the fluid are represented by the symbols α, β, ν, ρ, ΔT, respectively.

The heat transfer coefficient in terms of the local Nusselt number (Nu) is defined by the following expression:

$$Nu = Nu_l = Nu_r = Nu_b = Nu_s = -\frac{\partial\theta}{\partial n},$$

Where n denotes the normal direction on a plane.

while the average Nusselt number at the heated bottom wall, cold left and right walls and insulated top walls of the cavity is obtained as, $\overline{Nu}$ or $\mathrm{Nu}_{\mathrm{av}} = \int_0^1 Nu_l\,dX = \int_0^1 Nu_r\,dX = \int_0^1 Nu_s\,dX = \int_0^1 Nu_b\,dX$.

Stream function displays the fluid motion and is evaluated using the relationship between stream function ψ and velocity components U and V and defined as, $U=\dfrac{\partial\psi}{\partial Y}$ and $V=-\dfrac{\partial\psi}{\partial X}$ which yield a single equation, $\dfrac{\partial^2\psi}{\partial X^2}+\dfrac{\partial^2\psi}{\partial Y^2}=\dfrac{\partial U}{\partial Y}-\dfrac{\partial V}{\partial X}$. It is noted that anticlockwise circulation is denoted by $(+\psi)$ and clockwise circulation is represented by $(-\psi)$. Since no cross flow acts, so the no slip boundary is validated for all boundaries.

The heat flow within the cavity is displayed using the heat function (H) obtained from the conductive heat fluxes $\left(-\dfrac{\partial\theta}{\partial X},-\dfrac{\partial\theta}{\partial Y}\right)$ as well as convective heat fluxes $(U\theta,V\theta)$. The heat function satisfies the energy balance equation (equation 4), such that, $\dfrac{\partial H}{\partial Y}=U\theta-\dfrac{\partial\theta}{\partial X}$, $-\dfrac{\partial H}{\partial X}=V\theta-\dfrac{\partial\theta}{\partial Y}$ which yield a single equation $\dfrac{\partial^2 H}{\partial X^2}+\dfrac{\partial^2 H}{\partial Y^2}=\dfrac{\partial}{\partial Y}(U\theta)-\dfrac{\partial}{\partial X}(V\theta)$. Here the $(+H)$ denotes the anticlockwise heat flow and clockwise heat flow is represented by $(-H)$.

4 Numerical Procedure

COMSOL Multiphysics has been used to implement Galerkin weighted residual finite element method [24,25] and also the non-linear parametric solution method have been used to solve the mathematical dominant equations along with the specific boundary conditions for the current problem. A non-uniform triangular mesh arrangement has been implemented in the present research especially near the walls to capture the fast changes in the dependent variables. This approach will result in substantially fast convergence assurance.

To derive the finite element equations, the method of weighted residuals [26] is applied to the equations (1) – (4) as follows

$$\int_A N_\alpha \left(\frac{\partial U}{\partial X} + \frac{\partial V}{\partial Y} \right) \, dA = 0 \tag{5}$$

$$\int_A N_\alpha \left(U \frac{\partial U}{\partial X} + V \frac{\partial U}{\partial Y} \right) dA = -\int_A H_\lambda \left(\frac{\partial P}{\partial X} \right) dA + \Pr \int_A N_\alpha \left(\frac{\partial^2 U}{\partial X^2} + \frac{\partial^2 U}{\partial Y^2} \right) dA \tag{6}$$

$$\begin{aligned} \int_A N_\alpha (U \frac{\partial V}{\partial X} + V \frac{\partial V}{\partial Y}) dA = -\int_A H_\lambda (\frac{\partial P}{\partial Y}) dA + \Pr \int_A N_\alpha (\frac{\partial^2 V}{\partial X^2} + \frac{\partial^2 V}{\partial Y^2}) dA \\ + Ra \Pr \int_A N_\alpha \theta dA \end{aligned} \tag{7}$$

$$\int_A N_\alpha \left(U \frac{\partial \theta}{\partial X} + V \frac{\partial \theta}{\partial Y} \right) dA = \int_A N_\alpha \left(\frac{\partial^2 \theta}{\partial X^2} + \frac{\partial^2 \theta}{\partial Y^2} \right) dA \tag{8}$$

Where A is the element area, N_α (α = 1, 2, … …, 6) are the finite element interpolation functions for the velocity components and the temperature and H_λ (λ= 1, 2, 3) is the finite element interpolation functions for the pressure. Gauss's theorem is then applied to equations (6)-(8) to generate the boundary integral terms associated with the surface tractions and heat flux. Then equations (6)-(8) becomes,

$$\begin{aligned} \int_A N_\alpha \left(U \frac{\partial U}{\partial X} + V \frac{\partial U}{\partial Y} \right) dA + \int_A H_\lambda \left(\frac{\partial P}{\partial X} \right) dA \\ + \Pr \int_A \left(\frac{\partial N_\alpha}{\partial X} \frac{\partial U}{\partial X} + \frac{\partial N_\alpha}{\partial Y} \frac{\partial U}{\partial Y} \right) dA = \int_{S_0} N_\alpha S_x dS_0 \end{aligned} \tag{9}$$

$$\begin{aligned} \int_A N_\alpha (U \frac{\partial V}{\partial X} + V \frac{\partial V}{\partial Y}) dA + \int_A H_\lambda (\frac{\partial P}{\partial Y}) dA + \Pr \int_A (\frac{\partial N_\alpha}{\partial X} \frac{\partial V}{\partial X} + \frac{\partial N_\alpha}{\partial Y} \frac{\partial V}{\partial Y}) \\ - Ra \Pr \int_\alpha N_\alpha \theta dA = \int_{S_0} N_\alpha S_y dS_0 \end{aligned} \tag{10}$$

$$\int_\alpha N_\alpha (U \frac{\partial \theta}{\partial X} + V \frac{\partial \theta}{\partial Y}) dA + \int_\alpha (\frac{\partial N_\alpha}{\partial X} \frac{\partial \theta}{\partial X} + \frac{\partial N_\alpha}{\partial Y} \frac{\partial \theta}{\partial Y}) dA = \int_{S_w} N_\alpha q_{lw} dS_w \tag{11}$$

Here (9)-(10) specifying surface tractions (S_x, S_y) along outflow boundary S0 and (11) specifying velocity components and fluid temperature or heat flux (q_w) that flows into or out from domain along wall boundary S_w.

To find the result of the velocity and thermal energy, a set of non-linear coupled equations (1)-(4), for which an iterative scheme is adopted. The convergence of numerical solutions is assumed when the relative error for each dependent variable between consecutive iterations is recorded below the convergence criterion ε such that,

$$\sum \left| \psi_{ij}^{n} - \psi_{ij}^{n-1} \right| \leq \varepsilon ,$$

Where n is a number of iteration and $\Psi = U, V, \theta, P$ and $\varepsilon = 10^{-5}$; the indexes i, j indicate a grid point; and the index n is the current iteration at the grid level. The six node triangular element is used in this work for the development of the finite element equations. All six nodes are associated with velocities as well as temperature; only the corner nodes are associated with pressure. This means that a lower order polynomial is chosen for pressure. Quadratic interpolation is assumed by the element for the velocity components, the temperature distributions and linear interpolation for the pressure distribution according to their highest derivative orders in the differential equations (5) and (9) - (11) are presented as follows:

$$U(X,\ Y) = N_\alpha U_\alpha \tag{12}$$

$$V(X,\ Y) = N_\alpha V_\alpha \tag{13}$$

$$\theta(X,Y) = N_\alpha\ \theta_\alpha \tag{14}$$

$$P(X,\ Y) = H_\lambda\ P_\lambda \tag{15}$$

Where α = 1, 2, … …, 6; λ= 1, 2, 3; Substituting the element velocity component distributions, the temperature distribution, and the pressure distribution then from equations (12)-(15), the finite element equations can be written in the form,

$$K_{\alpha\ \beta}{}^{x} U_\beta + K_{\alpha\ \beta}{}^{y} V_\beta = 0 \tag{16}$$

$$K_{\alpha\beta\gamma}{}^{x} U_\beta U_\gamma + K_{\alpha\beta\gamma}{}^{y} V_\gamma U_\gamma + M_{\alpha\mu}{}^{x} P_\mu + \Pr\left(S_{\alpha\beta}{}^{xx} + S_{\alpha\beta}{}^{yy} \right) U_\beta = Q_\alpha{}^{u} \tag{17}$$

$$\begin{aligned} &K_{\alpha\beta\gamma}{}^{x} U_\beta V_\gamma + K_{\alpha\beta\gamma}{}^{y} V_\gamma V_\gamma + M_{\alpha\mu}{}^{y} P_\mu + \Pr(S_{\alpha\beta}{}^{xx} + S_{\alpha\beta}{}^{yy}) V_\beta \\ &- Ra \Pr K_{\alpha\beta} \theta_\beta = Q_\alpha{}^{v} \end{aligned} \tag{18}$$

$$K_{\alpha\beta\gamma}{}^{x} U_\beta \theta_\gamma + K_{\alpha\beta\gamma}{}^{y} V_\beta \theta_\gamma + \left(S_{\alpha\beta}{}^{xx} + S_{\alpha\beta}{}^{yy} \right) \theta_\beta = Q_\alpha \theta \tag{19}$$

Where the coefficients in element matrices are in the form of the integrals over the element area and along the element edges S_0 and S_w as,

$$K_{\alpha\beta^x} = \int_A N_\alpha N_{\beta,x} dA \quad , \quad K_{\alpha\beta^y} = \int_A N_\alpha N_{\beta,y} dA \quad , \quad K_{\alpha\beta\gamma^x} = \int_A N_\alpha N_\beta N_{\gamma,x} dA$$

$$K_{\alpha\beta\gamma^y} = \int_A N_\alpha N_\beta N_{\gamma,y} dA \quad , \quad K_{\alpha\beta} = \int_A N_\alpha N_\beta dA \quad , \quad S_{\alpha\beta^{xx}} = \int_A N_{\alpha,x} N_{\beta,x} dA$$

$$S_{\alpha\beta^{yy}} = \int_A N_{\alpha,y} N_{\beta,y} dA \quad , \quad M_{\alpha\mu^x} = \int_A H_\alpha H_{\mu,x} dA \quad , \quad M_{\alpha\mu^y} = \int_A H_\alpha H_{\mu,y} dA$$

$$Q_{\alpha^u} = \int_{S_0} N_\alpha S_x dS_0 \quad , \quad Q_{\alpha^v} = \int_{S_0} N_\alpha S_y dS_0 \quad , \quad Q_{\alpha\theta} = \int_{S_w} N_\alpha \, q_{1w} dS_w$$

$$Q_{\alpha\theta_s} = \int_{S_w} N_\alpha \, q_{2w} dS_w$$

These element matrices are evaluated in closed form for numerical simulation. Details of the derivation for these element matrices are omitted herein. Using the reduced integration technique of Reddy [17] and Newton–Raphson iteration technique by first writing the unbalanced values from the set of the finite element equations, the nonlinear algebraic equations (16)–(19) are modified by the imposition of boundary conditions. These modified nonlinear equations are transferred into linear algebraic equations using Newton's method. Finally, these linear equations are solved using Triangular Factorization method.

5 Grid Sensitivity Test

Grid sensitivity test is examined to find the appropriate number of grids and elements in a trapezoidal cavity with a non-uniformly heated triangular block (LBC) for Pr = 0.7, phi = 45° and Ra = 10^6. The following types of six different non-uniform grid systems of 6770, 9656, 13392, 17175, 21543, 26436 nodes and 992, 1436, 2007, 2589, 3261, 3968 elements were considered for the grid sensitivity tests. From these values, 17175 nodes and 2589 elements are adequate to produce an accurate result (Table 1).

Table 1. Grid Sensitivity Check at *Pr* = 0.7, *Phi* =45° *and Ra* = 10^6

Nodes (Elements)	6770 (992)	9656 (1436)	13392 (2007)	17175 (2589)	21543 (3261)	26436 (3968)
Nu	4.872581	4.872778	4.873732	4.87265	4.883798	5.071351
Time (s)	8.643	12.869	16.634	21.931	32.566	34.87

6 Code Validation

The present numerical algorithm is validated against the existing numerical results of Basak et al. [13] for a two-dimensional natural convection flow in a trapezoidal cavity having non-uniformly heated triangular block. The values of average Nusselt number (Nu_{av}) are anticipated for three different Rayleigh numbers (Ra = 10^3, 10^4 and 10^5) and also an angle ϕ = 0°, 30°, 45° as the Prandtl number is preset i.e., Pr = 0.7 for non-uniform heating of bottom wall. The obtained results are in good accord with those of Basak et al. [13] and are presented in Fig. 2.

7 Results and Discussion

Numerical research of natural convection flow in a trapezoidal cavity embedded inside a non-uniformly heated triangular block for different positions (LBC, RBC, LTC, and RTC) with non-uniform heating of bottom wall has been studied in this exertion. The results have been analysed for the case of the non-uniformly heated triangular block for diverse positions and also for heat transfer rates as well as local and

average Nusselt numbers. In addition, results are found for a wide range of parameters, such as Prandtl number, ($0.026 \leq Pr \leq 1000$) and Rayleigh number, ($10^3 \leq Ra \leq 10^6$) by way of various inclination angles, $\phi = 45^\circ, 30^\circ, 0^\circ$ (square cavity).

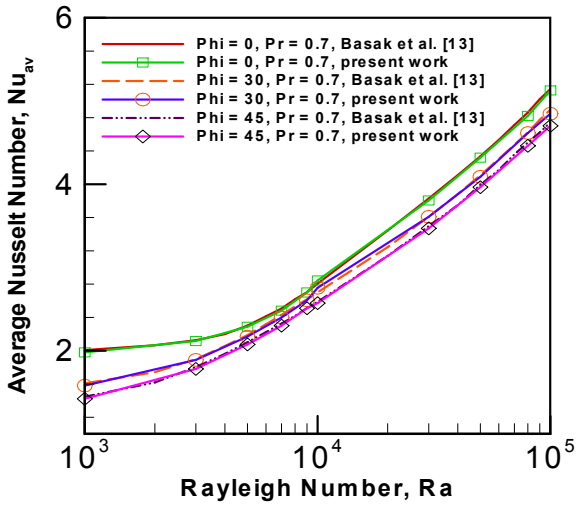

Fig. 2. Code validation for non-uniform heating of bottom wall with Pr = 0.7

7.1 Streamlines, isotherms, heatlines and pressures (For LBC triangular block)

Figs. 3-6 show the streamlines (stream functions), isotherms (temperature contours), heatlines (heat functions) and pressure contours for Rayleigh number, $Ra = 10^3 - 10^6$ and Prandtl number, Pr = 0.026-1000 (i.e. Pr = 0.026, 0.7, 1000) in the presence of non-uniformly heated bottom wall, cold side walls and well insulated top wall in a trapezoid cavity embedded inside a triangular solid body surface. The circulations of fluid strongly depend on non-uniformly heated triangular block (LBC) and also the parameters Pr and Ra. Due to heated triangular block and hot bottom wall, it has been seen that the fluid near to the hot bottom wall is hotter than the fluid near to the cold side walls. For this, the fluid close to the cold side walls has a larger density than the fluid near to the hot bottom walls. Consequently, from the middle portion of the bottom wall and also from the heated triangular block fluid rises up and flows down along the two side walls forming clockwise and anticlockwise rotations within the cavity.

Fig. 3 explains the streamlines (stream functions), isotherms, heat function and pressure contours for Pr =0.026, $Ra = 10^3$ for non-uniform heating of bottom wall within the cavity owed to the non-uniformly heated triangular block. In this case, symmetric primary circulations are seen in the cavity for low Rayleigh number ($Ra = 10^3$) and the worth of stream functions are considerably lesser with the inclination of ϕs. When $\phi = 0^0$(square cavity), the maximum value of stream function is $|\psi|_{max} = 0.7$. But for $\phi = 30^\circ$ and 45°, the maximum value of stream function is $|\psi|_{max} = 1.13$ and $|\psi|_{max} = 1.26$, respectively as seen in Figs. 3a-c. The isotherms with $\theta = 0.05 - 0.18$ occur symmetrically near the side walls of the cavity for $\phi = 0^\circ$ whereas, the isotherms by $\theta \geq 0.24$ are continuous curves. It means that a slightly stronger convection pushes the isotherms towards the walls. When $\phi = 30^\circ$, Pr = 0.026 and $Ra = 10^3$ then the isotherms with $\theta = 0.05 - 0.37$ occur symmetrically near the side walls of the cavity whereas, the isotherms by $\theta \geq 0.44$ are continuous curves (Fig. 3b). When $\phi = 45^\circ$, Pr = 0.026 and $Ra = 10^3$ then the isotherms with $\theta = 0.05$-0.44 are symmetric along the side walls and the other isotherms $\theta \geq 0.50$ are continuous curves and symmetric with respect to the vertical symmetrical line (Fig. 3c). By the intensity of circulations, $|\psi|_{max} = 0.7$ comparing to other cavities, it has been noted that the isotherms are high ($\theta = 0.95$) near to the non-uniformly heated

triangular block and hot bottom wall. The heatlines (heat function or total heat flux) are explained in panels (Fig. 3a-c). It is noted that heat flow via heatlines is symmetrically distributed along the cold side walls irrespective of ϕs. It is evident that isotherms with larger magnitudes for smaller ϕs towards the top portion of the side walls are opaque. It means that heatlines for ϕ = 0° is less dense than ϕ = 30° and 45°. Thermal boundary layer has been found to develop near the bottom edge as the heat transfer rate is quite large near to the non-uniformly heated triangular obstacle and also non-uniformly heated bottom wall. The pressure contours are also exemplified as shown in Fig. 3a-c. When ϕ = 0° (square cavity) then the pressure contours are linear. As the triangular block (LBC) and bottom wall are non-uniformly heated, the pressure contours are increasing from the middle portion of the bottom wall of the cavity and mostly dense in the edge of the heated triangular block. When ϕ = 0° then $|p|_{max}$ = 5 but for ϕ = 30° and 45° we have $|p|_{max}$ = 7.5 and $|p|_{max}$ = 8, respectively. Moreover, for ϕ = 30° and ϕ = 45° it is seen that the value of pressure contours is also increasing because of the smaller area and tough flow motions and seems to be bigger.

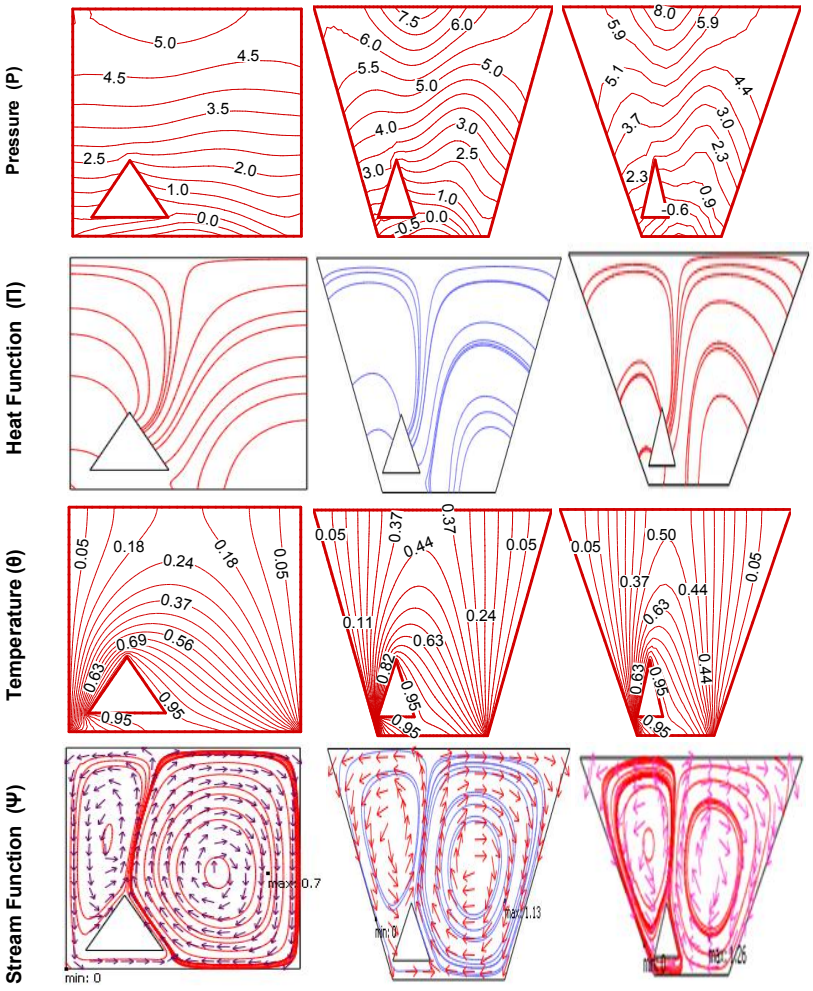

Fig. 3. Stream function (Ψ), temperature (θ), heat function (Π) and pressure (P) for LBC triangular block for non-uniform bottom heating θ(X,0) = sin(πx) with Pr = 0.026, and Ra = 10^3 where (a) ϕ = 0° (b) ϕ = 30° (c) ϕ = 45°

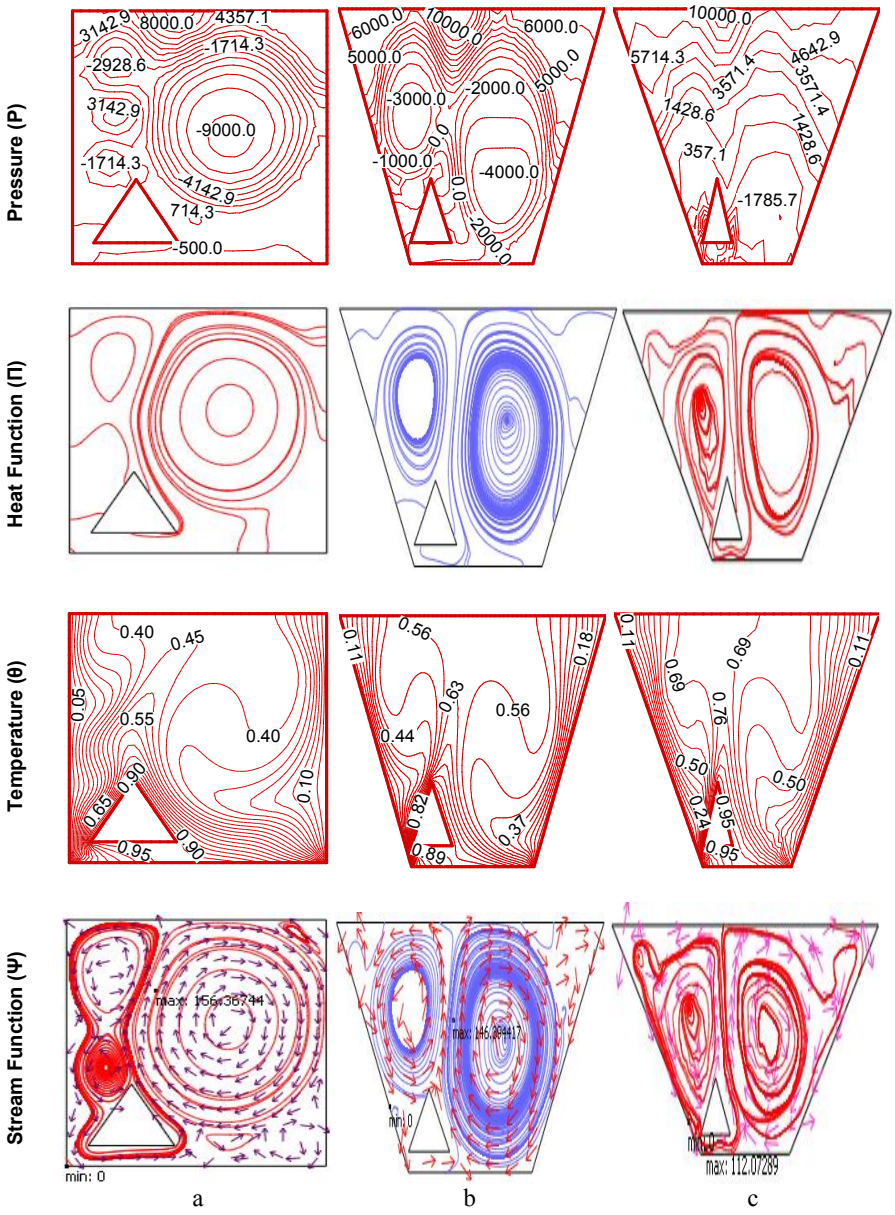

Fig. 4. Stream function (Ψ), temperature (θ), heat function (Π), pressure (P) for LBC triangular block for non-uniform bottom heating θ(X,0) = sin(πx) with Pr = 0.026, and Ra = 10^6 where (a) ϕ = 0° (b) ϕ = 30° (c) ϕ = 45°

At larger Rayleigh number (Ra = 10^6), the potency of circulations of the trapezoid swells by clockwise and anticlockwise rotations as seen in Fig. 4a-c. It has been observed that this critical Ra play a vital part for conveyance dominant form and the fluid flow strongly depends on Ra when Pr = 0.026 and also diverse angle of ϕs. It is interesting to note that two recirculation cells are formed and streamline plot is symmetric about the vertical midline due to the symmetry of the problem geometry. One cell is formed in the left side which looks like a tadpole and two more circular streamlines are also seen inside this ϕ = 0° (square cavity).

And the other cell looks like circular in the right. When the value of ϕ is increasing i.e. ϕ = 30° and 45° then the shapes of streamlines look like elliptical core because of enlarging of flow circulations and then also stream function´s magnitude $|\psi|_{max}$ are 156.36, 146.39 and 112.07 which implies reducing the position of the concentration of circulation. When Pr = 0.026 and Ra = 10^6 then the temperature contours θ ≤ 0.45, θ ≤ 0.63 and θ ≤ 0.76 are getting shifted towards the side walls. Then they break into two symmetric smooth contour lines and the isotherms with θ ≥ 0.45, θ ≥ 0.63 and θ ≥ 0.76 are at the evenhanded vertical line (see Fig. 4a-c). The temperature contours are condensed close to the side walls and also denser surrounded by non-uniformly heated triangular block. The flow intensity is stronger near to the centre of non-uniform heating of the bottom wall and LBC triangular block and weaker to the cold side walls and it does not go to the top wall as well shielded. There are two types of heatlines, which are illustrated in Fig. 4a-c. One indicates heat transfer from hot wall to cold walls and the other indicates the heat flow by the circulation cells of the fluid. The thermal boundary layer´s thickness seems to be huge for ϕ = 0° and correspondence to the less dense heatlines to the side walls whereas, heatlines are more condensed for ϕ = 30° and 45°. It is evident that heatlines are found to connect between two points of same side walls and the symmetric secondary heatline circulation cells are spanned by the non-uniform heating of LBC triangular block. Within the two cells, it is seen that two small circular heatline cells have found for ϕ = 0°, whereas, in case of ϕ = 30° and 45° the heatlines are elliptical interior by the transmission of motion. The stress contours are shown in Fig. 4a-c for Pr = 0.026 and Ra = 10^6. The shapes of circular contours of the stress of the trapezoid are seen for ϕ = 0° but due to heated triangular solid body surface smaller circular pressure contours are also seen in the left side implies flow circulation decreases. When ϕ = 30°, then it is evident that circulation of the left side is egg shaped and circulation of the right side is oval shaped and the flow circulations are oscillatory near the sides. We can also see the pressure contour circulations looks like wave shaped and its contours are the smaller amount by diminishing of movement of intensity.

When Prandtl number increases (Pr = 0.7) then for irrespective of ϕ = 0°, 30° and 45° and high Ra = 10^6 using LBC heated triangular block stream function, isotherms, heatlines and pressure contours have been discussed in Fig. 5. It is seen that when the values of angle increase then due to LBC obstacle and by the enhancing of fluid flow, two cells are formed for ϕ = 0° in the cavity while one cell is oval shaped situated in the left side and the other cell is like as pentagon. Streamlines are egg-shaped near the centre but also parallel near the side walls which exhibit the more strength of flow. Streamlines in the left side are denser than the right side in order to enhance heat transfer. But when ϕ increases for the trapezoid then streamlines are also denser for the two edges (left and right) because of the development of flow and thermal fields. Due to the wordiness principal heat transfer for Pr = 0.7 and Ra = 10^6 (see Fig. 5a-c) the temperature contours θ = 0.11 – 0.63, θ = 0.11 – 0.69 and θ = 0.11 – 0.63 are compressed asymmetrically along the walls and the isotherms θ ≥ 0.63, θ ≥ 0.63 and θ ≥ 0.69 are nearly even curves which span by the effect of LBC hot obstruct and from the middle of the bottom wall of the cavity and they are generally symmetric regarding upright symmetrical line. In case of superior circulation of the cavity, a little gradient in the temperature is noticed at the middle regime whereas a large stratification region of warmth is found at the even vertical line owing to the stagnation of surge. The intensity of heat circulation cells are magnified near to the region and heat transport is too found to be larger at the top portion of all ϕs. When Pr = 0 0.7 and Ra = 10^6, it has been noticed that, heatlines and streamlines are almost identical due to the superior intensity of flow at a large Pr. On the other side, heatlines are circular or elliptical for ϕ = 0°, Ra = 10^6 and Pr = 0.7. The denser heatlines with the centre vertical line represents the increased heat transfer for ϕ = 30° and 45° than ϕ = 0°. It is also seen that the maximum values of stream function are $|\psi|_{max}$ = 287.41, $|\psi|_{max}$ = 263.17 and $|\psi|_{max}$ = 256.96 for a variety of angles ϕ = 0^0, 30^0 and 45^0 which means heat surge is decreasing.

From Fig. 5a-c, it is observed that pressure are almost linear for ϕ = 0° than ϕ = 30° and 45°. From the middle portion of the non-uniform heating of the bottom wall of the trapezoid, the pressure contours come up and their value changes for the increasing of ϕs. The maximum values of pressure contours $|p|_{max}$ are 165714.3, 22000.0 and 200000.0 which happen through the help of augmenting of motion of flow.

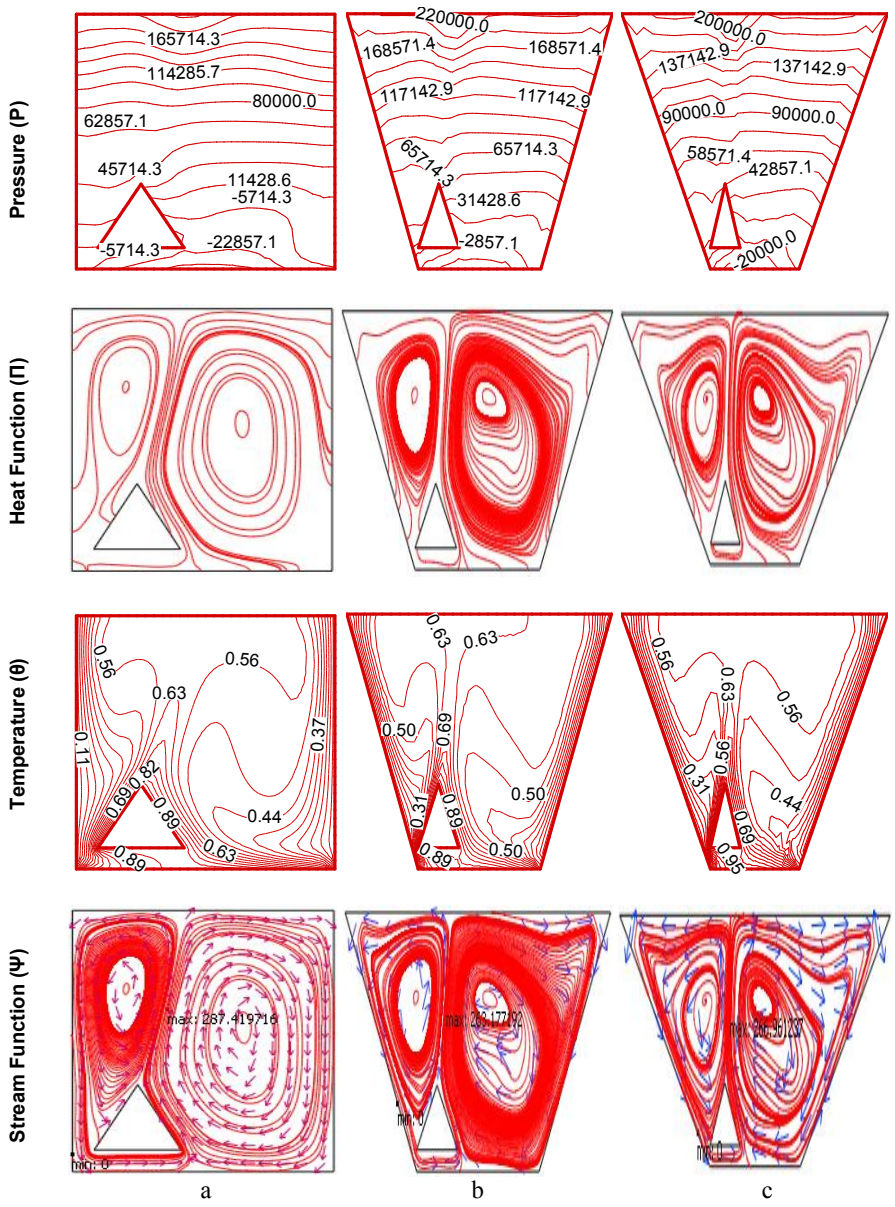

Fig. 5. Stream function (Ψ), temperature (θ), heat function (Π), pressure (P) for LBC triangular block for non-uniform bottom heating θ(X,0) = sin(πx) with Pr = 0.7, and Ra = 10^6 where (a) ϕ = 0° (b) ϕ = 30° (c) ϕ = 45°

At larger Pr = 1000 and Ra= 10^6 (see Fig. 6a-c), it is observed that intensity of circulation has been found to be further improved. The concentration of streamlines $|\psi|_{max}$ = 315.41 for ϕ = 0° and $|\psi|_{max}$ = 344.39 for ϕ = 30° and $|\psi|_{max}$ = 350.92 for ϕ = 45° are seen in Fig. 6a-c. By these values, it is illustrated that the intensity of convection is higher for high Pr. The isotherms with θ ≤ 0.63, θ ≤ 0.69 and θ ≤ 0.69 are highly compacted towards the side walls. The isotherms θ ≥ 0.63, θ ≥ 0.69 and θ ≥ 0.69 are non-stop curves with an innermost even symmetrical line for Ra = 10^6 and Pr = 1000. The heatlines (Fig. 6) are vastly thick for ϕ

= 30° and 45° than ϕ = 0° and cover the entire cavity and conquer the shape of the container. By the keenness of heat flood, two cells are seen at ϕ = 0° while heatlines seem to be circular or oval. When angles of trapezoid raise then the heatlines are more raising and a small vortex is made in the left side which is above the heated triangular block. However, for ϕ = 45° heatlines are denser than the other ϕs because of more intense flow. In addition, heatlines are less dense near the vertical portion of bottom wall by the reason of large gradient of heat function. The pressure contours are presented in Fig. 6a-c. It is messaged that pressures are almost linear for all irrespective ϕs. On account of more extreme circulation, the pressure contours are also increasing for ϕs, which are shown in Fig. 6a-c.

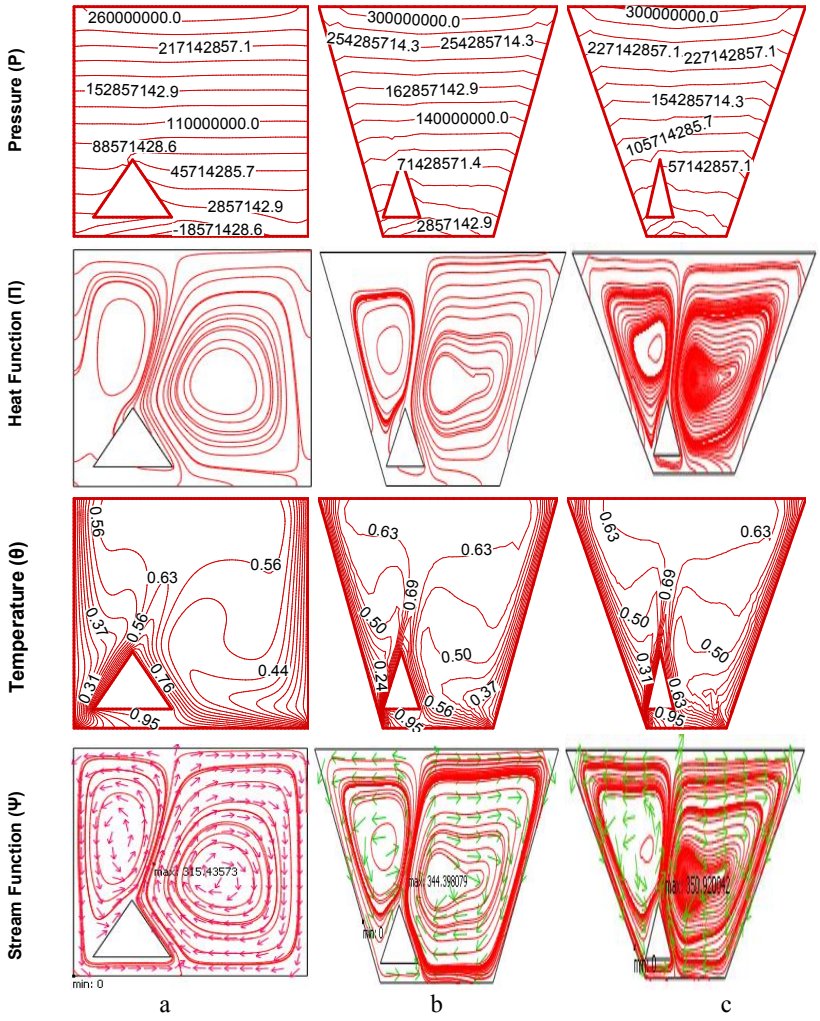

Fig. 6. Stream function (Ψ), temperature (θ), heat function (Π), pressure (P) for LBC triangular block for non-uniform bottom heating θ(X,0) = sin(πx) with Pr = 1000, and Ra = 10^6 where (a) ϕ = 0°(b) ϕ = 30° (c) ϕ = 45°

7.2 Streamlines, isotherms, heatlines and pressures (RBC triangular block)

Figs. 7 and 8 represent streamlines (stream function), isotherms, heatlines and pressure for Pr = 0.7 and Pr = 1000 respectively for higher Ra = 10^6 within a trapezoidal cavity entrenched inside a non-uniformly heated

RBC triangular block with the non-uniform heating of bottom wall for a wide range of inclination of angles ϕ. Fig. 7a-c illustrates that two cells are formed similar to LBC part. But here larger circulations of streamlines are situated in the right sides and smaller circulations are situated in the left side.

From Fig. 7a-c it is detected that the highest values of stream function are $|\psi|_{max}$ = 287.48, $|\psi|_{max}$ = 260.91 and $|\psi|_{max}$ = 255.17 for miscellaneous angles ϕ = 0°, 30° and 45° and Ra = 10^6 and Pr = 0.7 within the cavity. Because of vastly circulations, the streamlines are circular or elliptical alike to LBC branch. The isotherms amid θ ≤ 0.63, θ ≤ 0.76, θ ≤ 0.63 are compacted on the way to the side walls and the isotherms amongst θ ≥ 0.63, θ ≥ 0.76 and θ ≥ 0.63 are centrally symmetric for ϕ = 0° (square cavity), 30° and 45° and Ra = 10^6 and Pr = 0.7 . The heatlines for Pr = 0.7 are too alike as ϕ = 0°, 30° and 45° and Ra = 10^6 and Pr =0.026 (see Fig. 7a-c). One important feature is that heatlines reason to multiple flow circulation cells is observed for ϕ = 0°, 30° and 45° but thicker for ϕ = 30° and 45°.The pressure contours are seen as linear for dissimilar ϕs i.e. ϕ = 0°, 30° and 45° and when angle ϕ augments are caused by enhancing motions then the stress contours furthermore augment.

Fig. 8a-c shows the streamlines, isotherms, heatlines and pressures at larger Prandtl number (Pr = 1000) for non-uniformly heated RBC triangular block for diverse angles ϕ = 0°, 30° and 45° and Ra= 10^6. A prime role is played by the convection. The isotherms amid θ ≤ 0.63, θ ≤ 0.76, θ ≤ 0.69 are getting pushed in the direction of the side walls and the isotherms amongst θ ≥ 0.63, θ ≥ 0.76 and θ ≥ 0.69 come about symmetrically for Pr = 1000, Ra = 10^6 and ϕ = 0° (square cavity), 30° and 45° from non-uniform heating of the bottom wall with the effect of RBC triangular obstruct. It may be noted that, greatest value of stream function is $|\psi|_{max}$ = 363.20 for ϕ = 45^0(see Fig. 8a-c). The heatlines are alike as previous (Fig. 7a-c). In order to non-uniformly heated RBC triangular solid body surface, one small egg shaped eddy and one small elliptical are seen in the left and right side respectively, for ϕ = 30°. The heatlines are exceedingly darker for ϕ = 45° cause to high forceful flow. The pressure contours (see Fig. 8a-c) for Pr = 1000 are parallel to before Pr = 0.7 and Ra = 10^6 (see Fig. 7a-c). Because of more circulations of the stream, the highest values of pressure are seen for ϕ = 45° in the cavity.

7.3 Streamlines, isotherms, heatlines and pressures (For LTC triangular block)

Figs. 9 and 10 demonstrate the streamlines, temperature contours, heatlines and pressure for the different values of parameters Pr = 0.7 and 1000 for highest Rayleigh number (Ra = 10^6) with various inclination angles ϕ = 0°, 30° and 45° for the non-uniformly heated the triangular block (LTC). It is studied that due to triangular block two cells, such as, left and right are formed in the cavity. The behaviour occurs by the values of thermal conductivity. One primary eddy is made in the left side belonging LTC part and secondary eddy is made in the right side. Streamlines are circular or elliptical ϕ = 0°, 30° and 45° and darker for ϕ = 30° and 45° and streamlines are thicker for ϕ = 0° (square cavity) than ϕ = 30°, 45° (see Fig. 9 a-c), at the same time as, streamlines are also thicker ϕ = 30° (see Fig. 10 a-c) contained by the cavity. This happens due to the intensity of fluid flow fields inside the cavity. By the activity of the fluid, the maximum values of ψ are recorded as, $|\psi|_{max}$ = 233.56 for Pr = 0.7, Ra = 10^6 and ϕ = 0° (square cavity) (see Fig. 9 a-c), whereas, $|\psi|_{max}$ = 233.56 for PR = 1000, Ra = 10^6 and ϕ = 0° (square cavity) (see Fig. 10a-c) in the trapezoid cavity. It is clear that a good convection is obtained and fluid flows strongly inside the cavity.

Isotherms = 0.1 - 0.5 occur symmetrically near the side walls of the cavity ϕ = 0° (Fig. 9a-c). The other isotherms θ ≥ 0.6 are smooth curves symmetric with respect to vertical symmetrical line at the centre and θ ≤ 0.9 are also continuous curves. These are also symmetric around the LTC triangular block (Fig. 9a-c) and also smooth curves around LTC triangular obstruct for Ra = 10^6, ϕ = 30°, 45° when Pr = 0.7. This is also exactly calculated for Ra = 10^6, ϕ = 0°, 30°, 45°, when Pr = 1000 (Figs. 9, 10). Isotherms are stronger and more condensed asymmetrically around the triangular block and also near the side walls attributable to stronger primary movement cell. The heatlines are spherical for ϕ = 0° (see Fig. 9) and more dense in the

centre of the left side whereas heatlines seem to be oval for ϕ = 30°, 45° (Fig. 9b-c) and less dense than others. One small elliptical eddy recirculations are seen in the left side while the shape of heatlines in the right side of the cavity seems to be embryo (Fig. 9). It has been also found that secondary eddy is formed above of the heated triangular block for heatlines and also streamlines for Pr = 1000, Ra = 10^6 and a wide range of ϕ (Fig. 10). It is analysed that pressure contours are linear from the middle to the top portion of the cavity and non-linear in the side of the bottom wall (Fig. 9) whilst pressure contours are just about linear in the trapezoidal cavity (Fig. 10). The value of pressure contours increases when the angle ϕ increases, but also for less area of the cavity and also high heating flow effects.

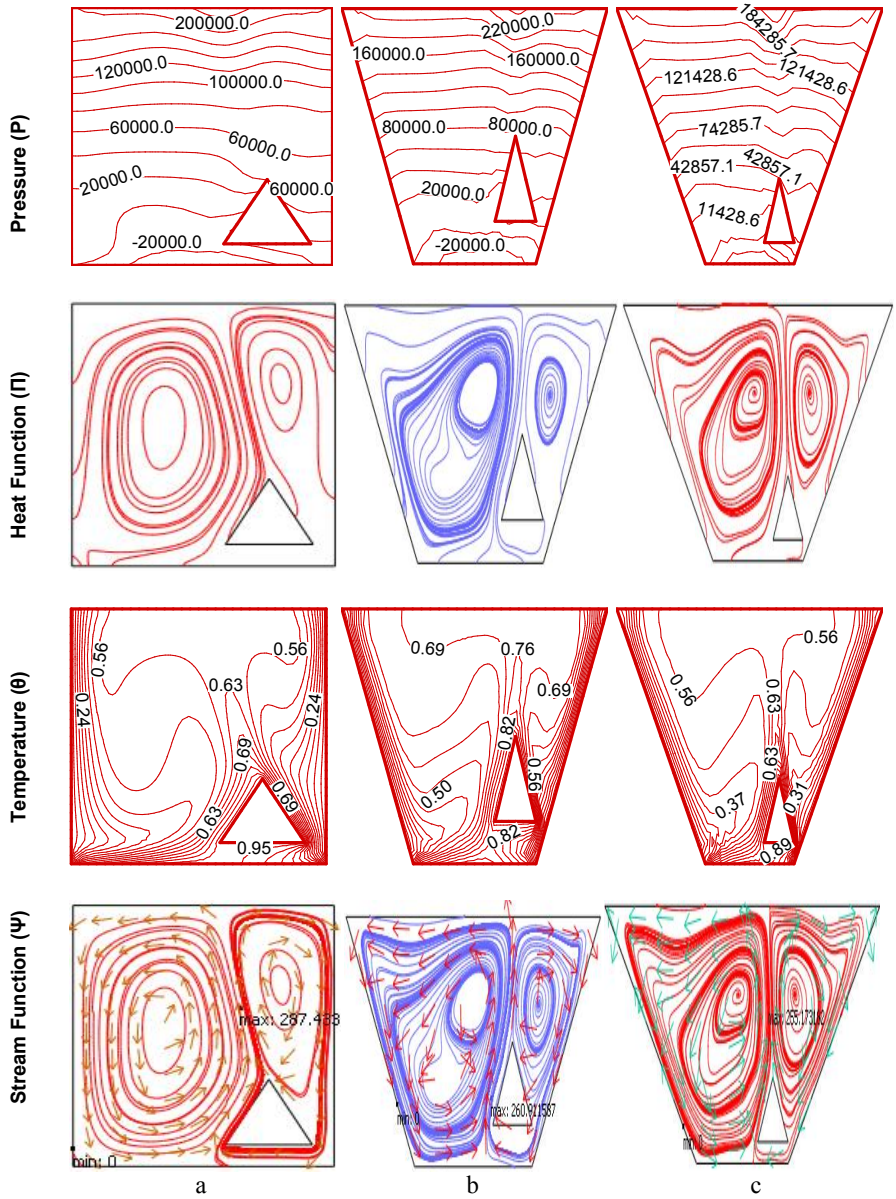

Fig. 7. Stream function (Ψ), temperature (θ), heat function (Π), pressure (P) for RBC triangular block for non-uniform bottom heating θ(X, 0) = sin(πx) with Pr = 0.7, and Ra = 10^6 where (a) ϕ = 0° (b) ϕ = 30° (c) ϕ = 45°

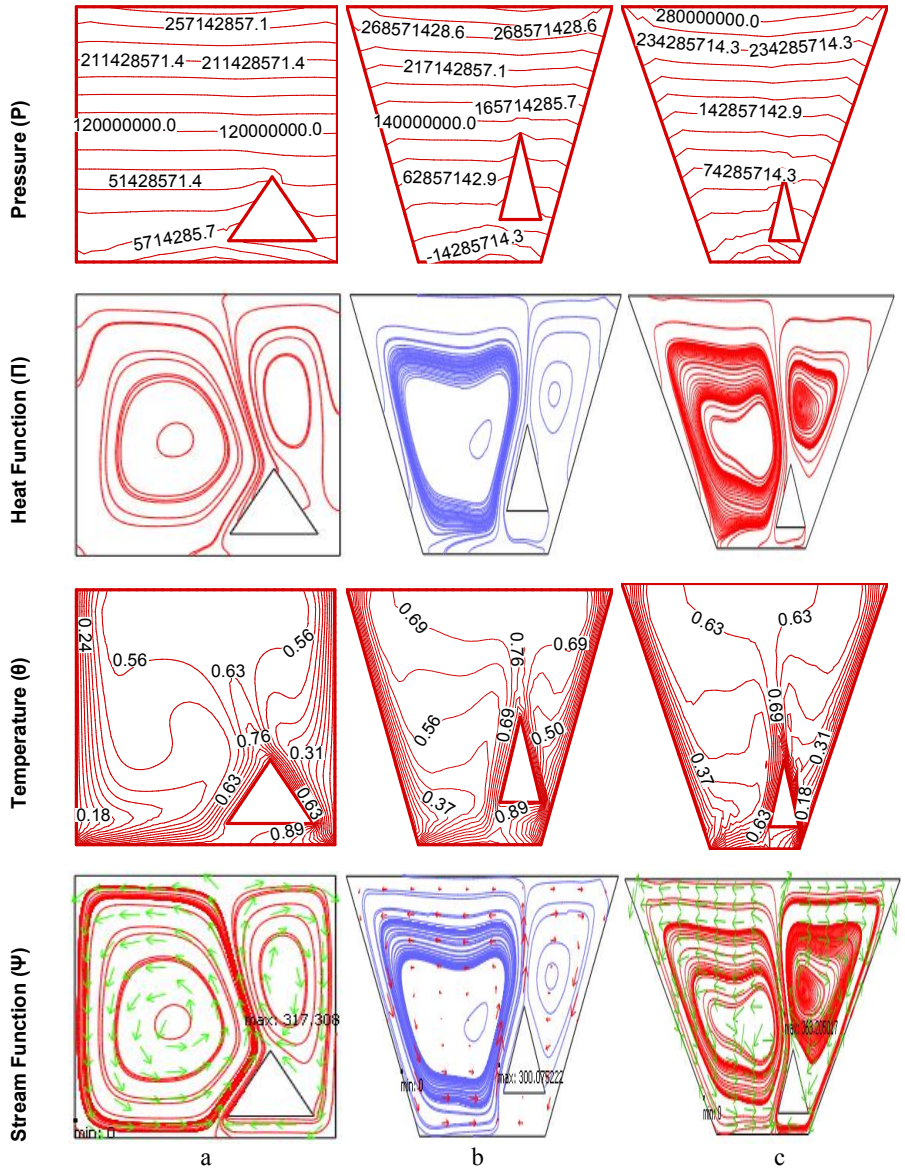

Fig. 8. Stream function (Ψ), temperature (θ), heat function (Π), pressure (P) for RBC triangular block for non-uniform bottom heating θ(X, 0) = sin(πx) with Pr = 1000, and Ra = 10^6 where (a) ϕ = 0° (b) ϕ = 30° (c) ϕ = 45°

7.4 Streamlines, isotherms, heatlines and pressures (For RTC triangular block)

Figs. 11-12 put emphasis on the streamlines, isotherms, heatlines and pressures for Pr = 0.7, 1000 for an assortment of liking angles ϕ surrounded by the RTC triangular wedge in a trapezoidal cavity. In order to non-uniformly heated RTC triangular block, it has been noticed in the left side that, one eddy is fruit shaped like mango for ϕ = 0°, Pr = 0.7 and 1000. Besides, the elliptical distribution is found for Pr = 0.7 and 1000 within this eddy. When Pr = 0.7, one tiny secondary vortex is seen at the north-east corner of RTC block and three secondary eddies with multiple, is circular also seen below the triangular block for ϕ = 0° (Fig. 11a). Similarly it happens for Pr = 1000 and ϕ = 0° (Fig. 12a). When ϕ increases then bucket type of eddy is made

in the left side of the trapezoid cavity (Fig. 11 b-c, 12b-c) for ϕ = 30° and 45° and one egg shaped secondary vortex is seen at the north-east corner of the RTC triangular block (see Fig. 11, 12c). Besides this, one tiny circular shape is founs within the oval at the north–east corner (Fig. 12c). Streamlines are denser for ϕ = 0° and Pr = 0.7 although streamlines are denser for ϕ = 0° and 30° when Pr = 1000. When Pr = 0.7 then $|\psi|_{max}$ = 230.76, $|\psi|_{max}$ = 211.04 and $|\psi|_{max}$ = 193.30 for Ra = 10^6 and different ϕs. Also is further enhanced for Pr = 1000 and then the maximum values of stream function by the advanced intensity of flow are $|\psi|_{max}$ = 258.91, $|\psi|_{max}$ = 258.56 and $|\psi|_{max}$ = 244.66 for Ra = 10^6 and dissimilar ϕs i.e. ϕ = 45°, 30°, 0° (square cavity).

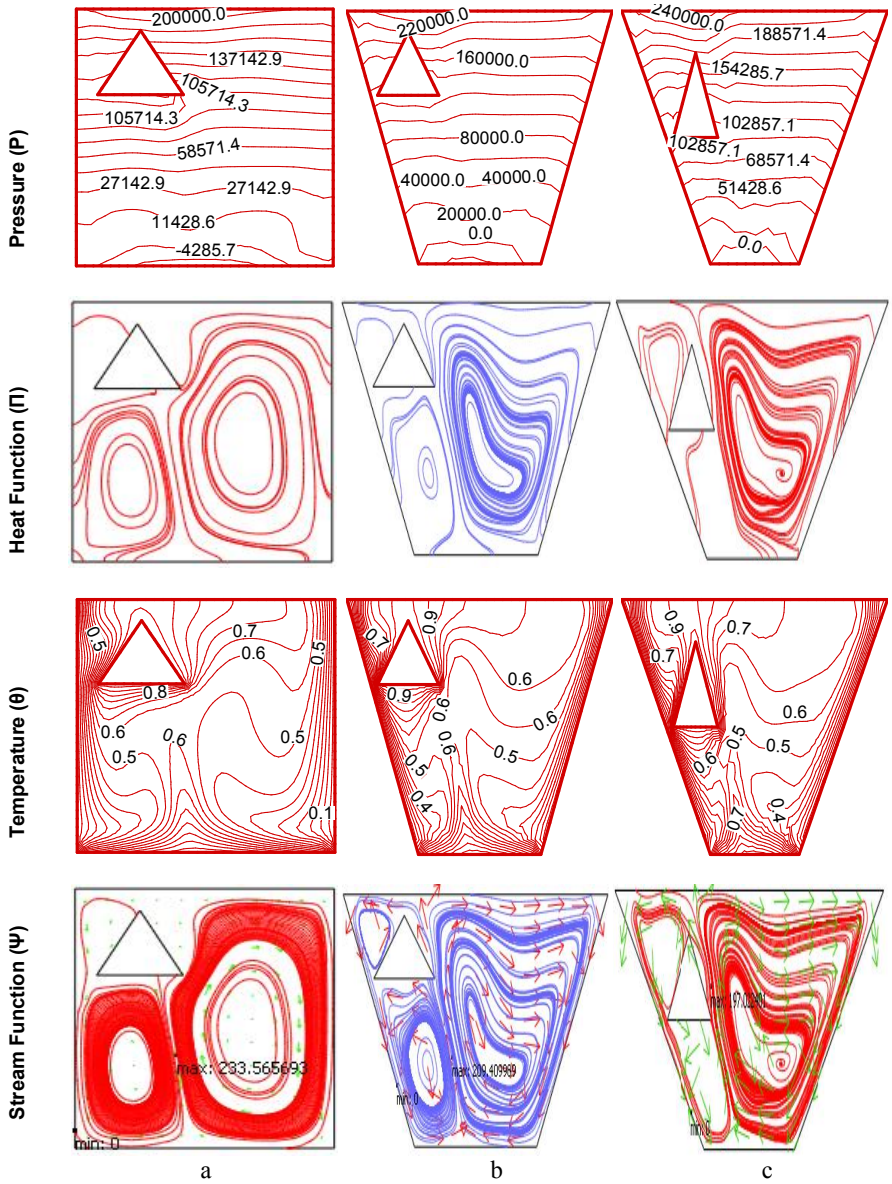

Fig. 9. Stream function (Ψ), temperature (θ), heat function (Π), pressure (P) for LTC triangular block for non-uniform bottom heating θ(X, 0) = sin(πx) with Pr = 0.7, and Ra = 10^6 where (a) ϕ = 0° (b) ϕ = 30° (c) ϕ = 45°

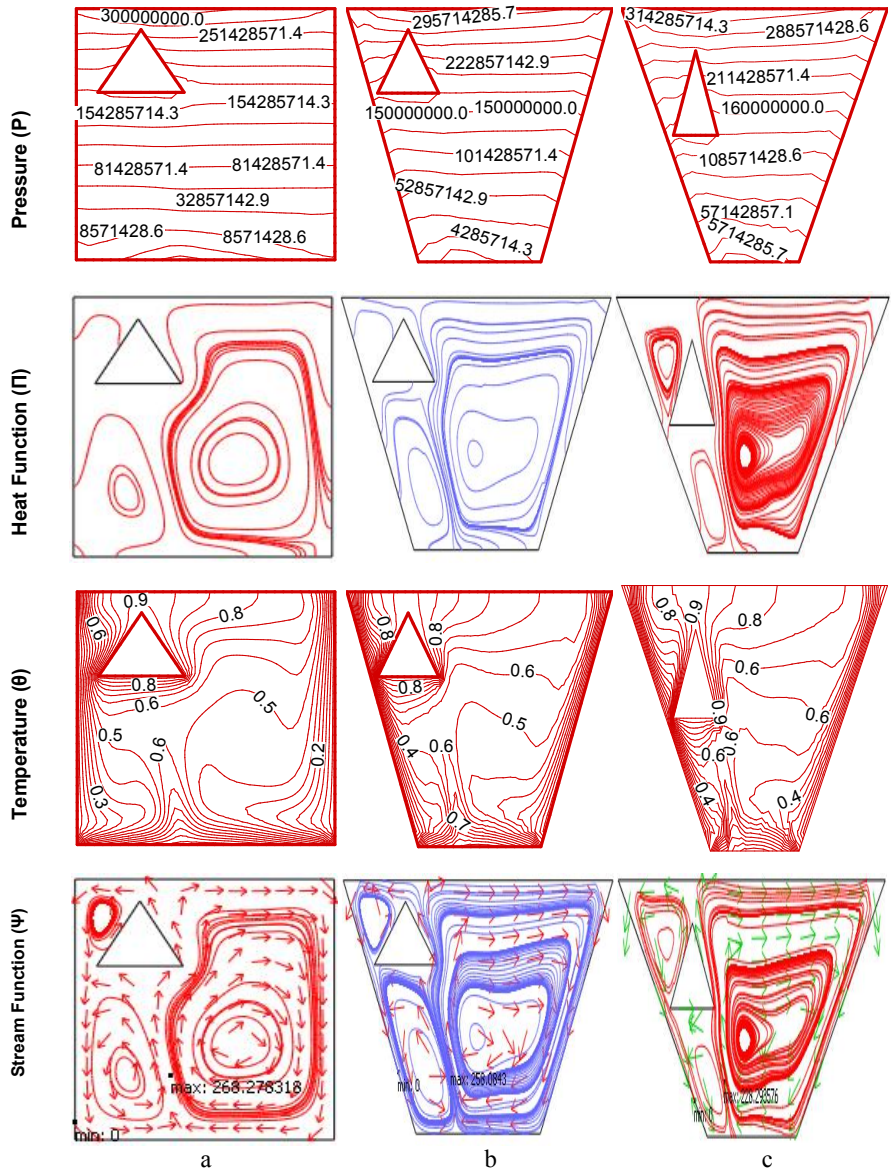

Fig. 10. Stream function (Ψ), temperature (θ), heat function (Π), pressure (P) for LTC triangular block for non-uniform bottom heating θ(X,0) = sin(πx) with Pr = 1000, and Ra = 10^6 where (a) ϕ = 0° (b) ϕ = 30° (c) ϕ = 45°

The results have been further examined with isotherms for lower to higher Prandtl number. Isotherms are created to be extremely compressed with θ = 0.1 - 0.5 owing to enlarge fluid circulations. The isotherms θ ≥ 0.6 are continuous curves regarding vertical symmetrical line at the centre of the bottom wall and also symmetric in the region of non-uniformly heated RTC triangular block for Pr = 0.7 and 1000 with mixed leaning angles ϕ = 0°, 30° and 45° and Ra = 10^6 (see Fig. 11-12). It has been observed that thickness of thermal boundary layers is denser at north-east portion of RTC triangular block for Pr =1000 as compared to Pr = 0.7.

It is also remarked that the shapes of stream functions are just about trapezoid in the neighbourhood of the wall of a bigger amount of fluid circulations and signifies the boosting thermal mixing results. At higher

Rayleigh number (Ra = 10^6) and higher Prandtl number (Pr = 1000), heatlines cover the entire cavity and attain the shape of the container i,e. circular, oval or trapezoidal for ϕ = 30^0 and 45^0 (see Figs. 11-12). Besides this, heatlines are less dense near the bottom section of vertical walls and depth of boundary level is larger at the bottom portion of the side walls and heatlines are also denser through several circulations for Pr = 0.7 and ϕ = 45º, 30º (Fig. 11 b-c) and too for ϕ = 45º, 30º when Pr = 1000. From the panels of Figs. 11-12, it is noticed that the pressure contours are linear for Pr = 0.7 and 1000 and on account of enhancing manifold fluid circulations, the values of pressure contours increases at higher Prandtl number, Pr = 1000.

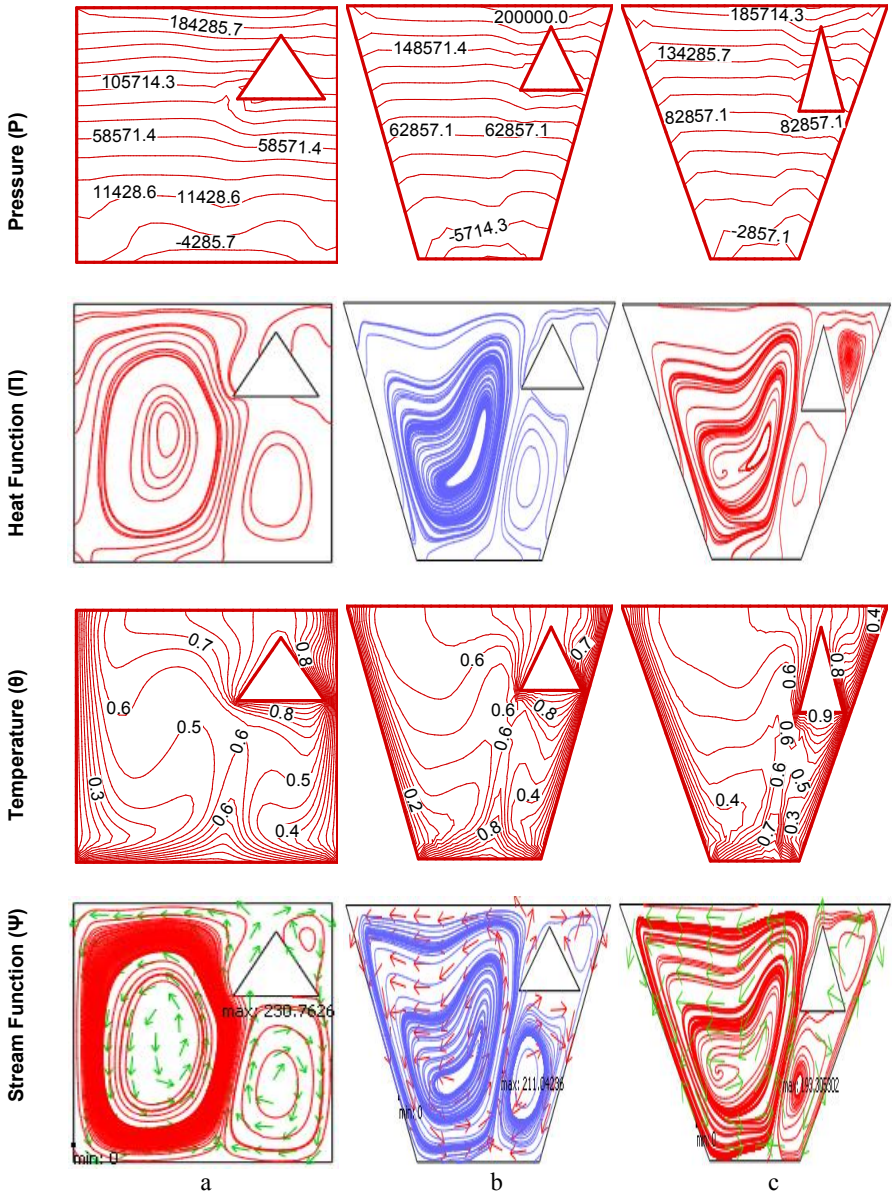

Fig. 11. Stream function (Ψ), temperature (θ), heat function (Π), pressure (P) for RTC triangular block for non-uniform bottom heating θ(X, 0) = sin(πx) with Pr = 0.7, and Ra = 10^6 where (a) ϕ = 0° (b) ϕ = 30° (c) ϕ = 45°

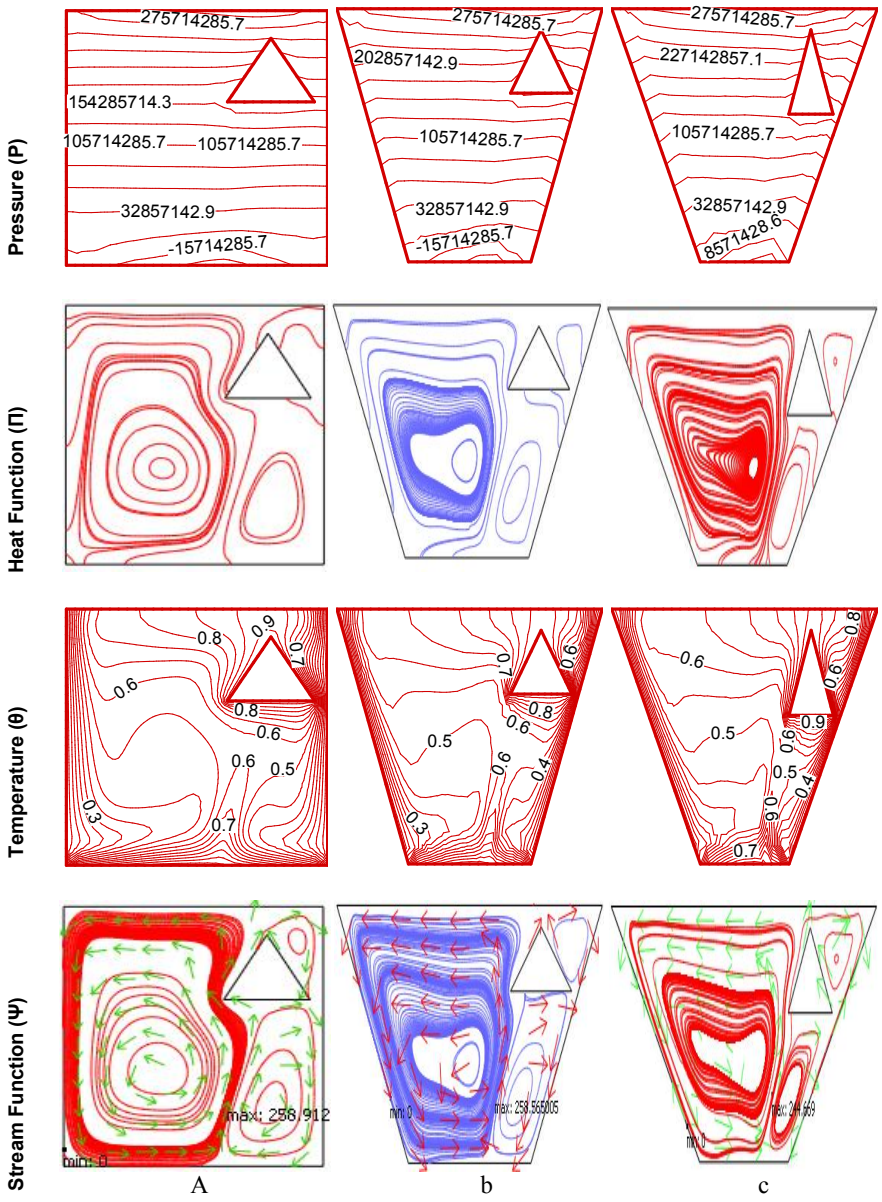

Fig. 12. Stream function (Ψ), temperature (θ), heat function (Π), pressure (P) for RTC triangular block for non-uniform bottom heating θ(X,0) = sin(πx) with Pr = 1000, and Ra = 10^6 where (a) ϕ = 0° (b) ϕ = 30° (c) ϕ = 45°

7.5 Heat transfer rates: Local nusselt number vs distance

Fig. 13 illustrates the local Nusselt number vs distance for Pr = 0.026 with a range of tilt angles ϕ = 0°, 30°, 45° and Ra = 10^3 for a non-uniformly heated triangular block for different positions (LBC, RBC, LTC, RTC) which occurs inside the cavity. As the physical conditions of the cavity follow the non-uniformly heated bottom wall, cooled left and right (side) wall and insulated top wall and too LBC non-uniformly hot triangular block inside the cavity, so that, maximum heat transfer rates of local Nusselt number are seen near the edge of the side wall. Then it is moving with the angle direction due to LBC heated triangular obstruct

and shows the minimum heat transfer rates of local Nusselt number near the west-south corner position and afterwards it also moves to the right side. Since the Rayleigh number is the multiple of Grashof number and Prandtl number, accordingly, the heat transfer rates change the cause of Grashof number as Prandtl number is preset. It is forestated that the heat transfer rates for $\phi = 0^{\circ}$, 30°, $\phi = 45^{\circ}$ are almost same for $Ra = 10^3$ and $Pr = 0.026$. Besides, as non-uniformly heated triangular block stays inside the right side of lower part of the cavity i.e., for RBC, it is seen that the heat transfer rate is minimum near the south-east position of bottom wall and the rate is maximum near the edge of the side (left and right) wall for $Pr = 0.026$ and $Ra = 10^3$. The heat transfer rates loosely change for $Ra = 10^3$. It has been noticed that when ϕ increases then the heat transfer rate decreases. Since triangular block effects the cavity in the left top side then it is discovered that heat transfer rate of local Nusselt number is minimum in the left (side) and near the bottom edge of the wall and maximum near the edges of the wall due to transmission dominant system for $Ra = 10^3$ when $Pr = 0.026$. Also for the RTC triangular block found that heat transfer rates are maximum near the side wall and minimum close to the right wall and bottom edge of the wall for a range of inclination angles $\phi = 0^{\circ}$, 30°, 45° and $Ra = 10^3$ when $Pr = 0.026$.

Fig. 14 depicts that when Ra increases ($Ra = 10^6$) then the heat transfer rates of local Nusselt number increases for $\phi = 30^{\circ}$ and decreases for $\phi = 0^{\circ}$ to the south–east corner position of the right side as convection is overriding for higher Ra due to non-uniformly heated LBC triangular obstacle. Besides in presence of non-uniform heating of RBC triangular obstacle, the heat transfer rates changes more for $Ra = 10^6$, which means the central regime is observed. Also for LTC, when $Ra = 10^6$ and $Pr = 0.026$, the heat transfer rate goes up and down and moving because of less non-uniform heating of the bottom wall. It is also watched that heat transfer rate is found to be minimum near the bottom edge of the right wall and preceding effects happen in the case of maximum. Besides this, a little change of heat transfer rates with the distance from 0.1-0.3 is seen due to the presence of thermal boundary conditions in LTC figure. But owing to RTC figure it has been found that the heat transfer rate changes are taking at distances from 0.3-0.5 for high $Ra = 10^6$.

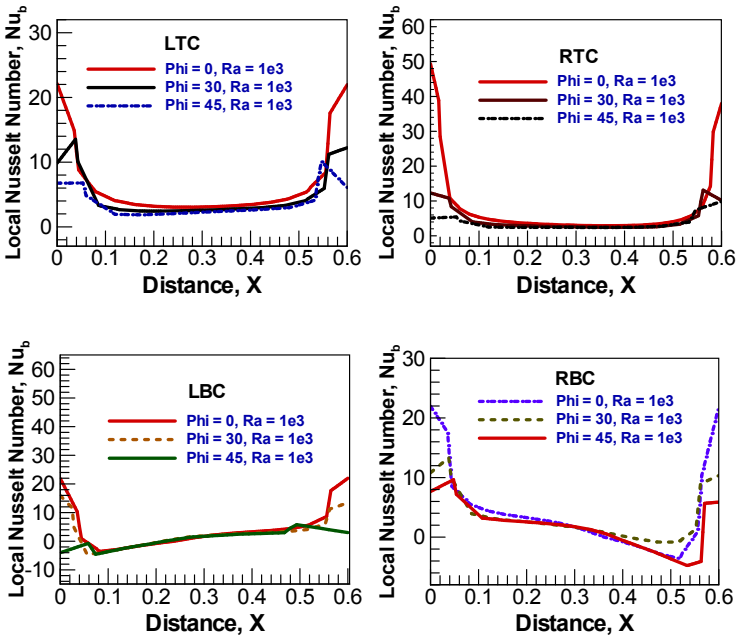

Fig. 13. Variations of local Nusselt numbers (Nu_b) with distance for $Pr = 0.026$, $Ra = 10^3$ and for various inclination of angles $\phi = 0°, 30°, 45°$ in presence of non-uniform heating of LBC, RBC, LTC, RTC triangular block

When Pr increases to 0.7 then a little discontinuity is found near west-south edge of the bottom wall and also near the south-east edge of the right wall which occurs owing to non-uniformly heated LBC triangular block for Ra = 10^6 (Fig. 15). It is also analysed from the non-uniformly heated RBC triangular block that the temperature contours near the bottom edge of cold side (left and right) walls are mostly compressed due to the discontinuity right edge resulting in high thermal gradient near the right edge of the bottom wall. But for Pr = 0.7 and Ra = 10^6 it has been observed that heat transfer rate is minimum near to the bottom edge with distance 0.2-0.3 to near the middle position and discontinuity presents near the corner edge of the wall cause to the LTC triangular block. Because of discontinuity, the heat transfer rate is very high at the edges of these two sides. It has been also noticed that the intensity of both primary and secondary cells at higher for Ra = 10^6 and consequently the temperature contours start to shift from bottom wall towards the side wall and also for high Ra= 10^6 the heat transfer rate has been changed taking distances from 0.3-0.48 in the RTC figure.

Due to increase of strength of circulations the heat transfer rates are larger for Pr = 1000 and also Ra = 10^6 and the heat transfer rates for local Nusselt number slightly changes for $\phi = 0^\circ$ except $\phi = 30^\circ$ and 45° in the middle position of the bottom wall which is seen in LBC part of Fig. 16. For Pr = 1000 and Ra = 10^6 it has been seen that the magnitudes of the heat transfer rates also increase in RBC figure. The heat transfer rate at the bottom edge of the wall is zero which starts from the left side and a decreasing movement in Nu_{local} is viewed from the bottom edge to the top edge of the right wall. Due to enlarge viscous effect Pr increases to 1000, so, the power of both primary and secondary circulations and the temperature contours are compacted in the direction of the top portion of the left wall for unlike irrespective ϕs. In case of LTC figure, same effects are happening like the previous one (Fig. 15). When Prandtl increases (Pr = 1000), it has been noticed that heat transfer rate is minimum between near bottom edge of the wall with distance 0.35-0.48 and right (side) for Ra = 10^6 and various ϕs, which occurs in order to strength flow circulations for non-uniform heating of RTC triangular block. The discontinuity position also holds within this distance. The heat transfer rates usually decrease for the left wall and then increase to the right wall. Hence at higher Rayleigh number and higher Prandtl number, the heat transfer rates are magnified at the regimes from the bottom corner points.

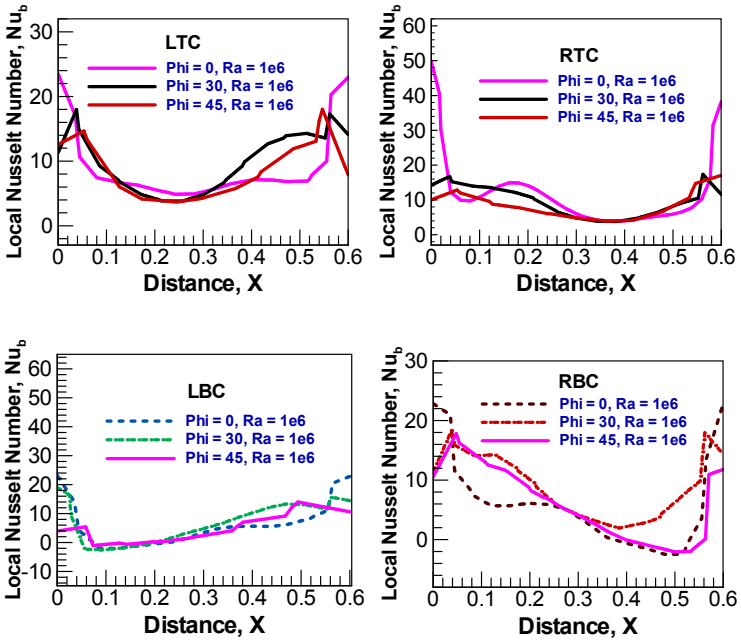

Fig. 14. Variations of local Nusselt numbers (Nu_b) with distance for Pr = 0.026, Ra = 10^6 and for various inclination of angles $\phi = 0°, 30°, 45°$ in presence of non-uniform heating of LBC, RBC, LTC, RTC triangular block

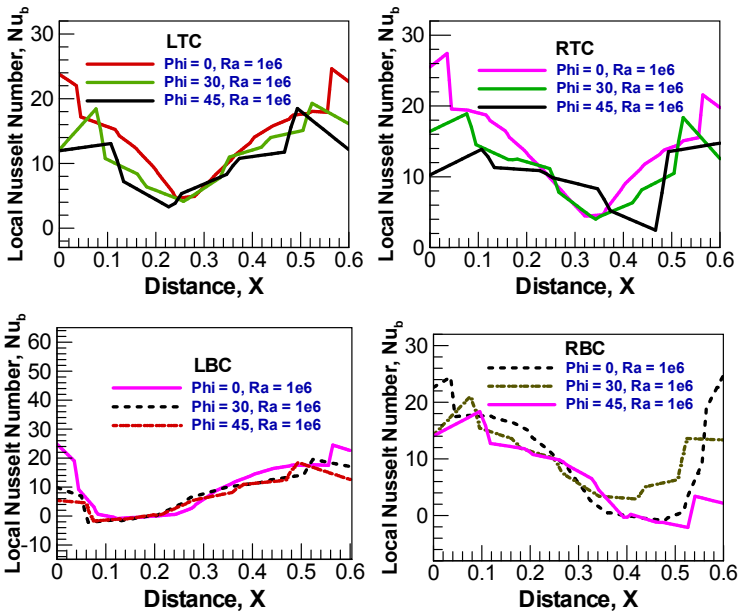

Fig. 15. Variations of local Nusselt numbers (Nu_b) with distance for Pr = 0.7, Ra = 10^6 and for various inclination of angles ϕ = 0°, 30°, 45° in presence of non-uniform heating of LBC, RBC, LTC, RTC triangular block

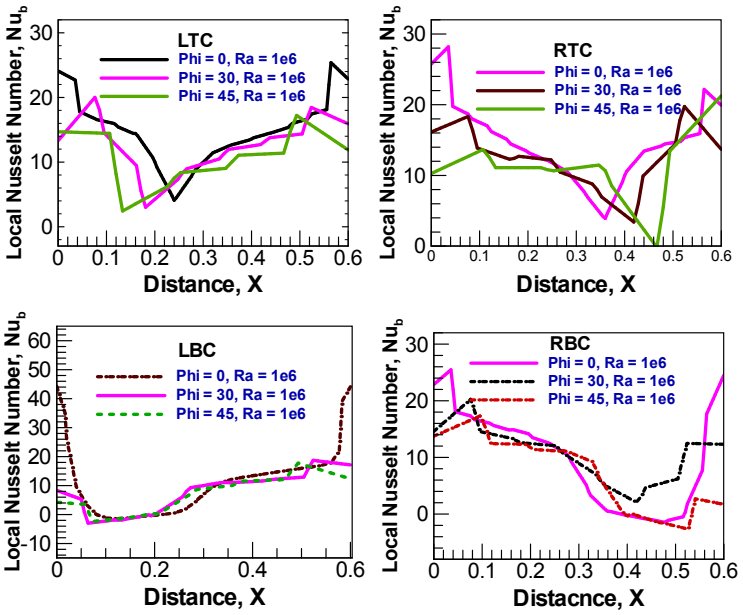

Fig. 16. Variations of local Nusselt numbers (Nu_b) with distance for Pr = 1000, Ra = 10^6 and for various inclination of angles ϕ = 0^o, 30^o, 45^o in presence of non-uniform heating of LBC, RBC, LTC, RTC triangular block

7.6 Heat transfer rates: Average nusselt number vs rayleigh number

The heat transfer performance in terms of average Nusselt number (Nu_{av}) with the help of non-uniformly heated triangular block for different positions (LBC, RBC, LTC, RTC) inside the trapezoidal cavity in Fig. 17 a-c are displayed for (a) Pr = 0.026, (b) Pr = 0.7 and (c) Pr = 1000 and also for various leaning angles ϕ = 0^o, 30^o and 45^o. Fig. 17 a-c also show the distributions of the average Nusselt number of non-uniform heating of the bottom wall which has been analysed by plotting against Rayleigh number. Based on heat lines via total heat flux or heatlines, the average Nusselt number has been calculated using temperature gradient. It may be noted from Fig. 17 a-c (LBC) that, when the angle ϕ increases then average Nusselt number decreases but when Rayleigh number (Ra) increases then average Nusselt number increases. It is seen from Fig. 17a (LBC) that, heat transfer rate of average Nusselt number swiftly reaches from ϕ = 30^o to ϕ = 0^o, in order to conduction dominant heat transfer for Pr = 0.026. But Nu_{av} is swiftly increasing at the higher Rayleigh number when Pr increases from 0.7 to 1000, which is seen in Fig. 17b-c (LBC).

For LBC, it is also seen that Nu_{av} are almost identical for ϕ = 30^o and 45^o except ϕ = 0^o for higher Pr = 0.7 and 1000 (See Fig. 17 b-c). From RBC, it is observed that average Nusselt number for ϕ = 30^o is higher than ϕ = 0^o due to the huge intensity of flow when Pr = 0.026. It is also observed that Nu_{av} are straightly moving for Ra = 10^3 to near Ra = 10^5 and for ϕ = 0^o and 30^o but at Ra = 10^5, average Nusselt number intersects each other for Φ = 0^o and 30^o except ϕ = 45^o and then increases swiftly between Ra = 10^5 to Ra = 10^6 taking identically distribution for increasing Pr from 0.7 to 1000, which occurs for highly viscous of Pr. Similar distribution of heat transfer rates for the average Nusselt number are also exhibited for (Fig. 17b-c) (LTC) for ϕ = 0^o, 30^o and 45^o and also for Pr = 0.7 and 1000. But when Pr = 0.026 in LTC then the heat transfer rates for Nu_{av} are compressed significantly at a higher value of Ra = 10^6. This confirms that the heat transfer is also staying in conduction dominant mode for Prandtl number, Pr = 0.026. From Fig. 17a-c (RTC), it is obvious that the higher value of the heat transfer rate of Nu_{av} is found for increasing Ra irrespective of ϕs. But it has been also noticed that the average Nusselt number swells a little for Pr = 0.026 and for higher Ra but for higher Pr it is originated that Nu_{av} is also quickly elevating for higher Ra. It is also eminent from Figs. 17 a-c (LBC, RBC, LTC, RTC) that decreasing situation of Nu_{av} remains invariant irrespective of ϕs of Pr at higher Ra. The magnitudes of average Nusselt number are found to be lower due to the non-uniform heating case.

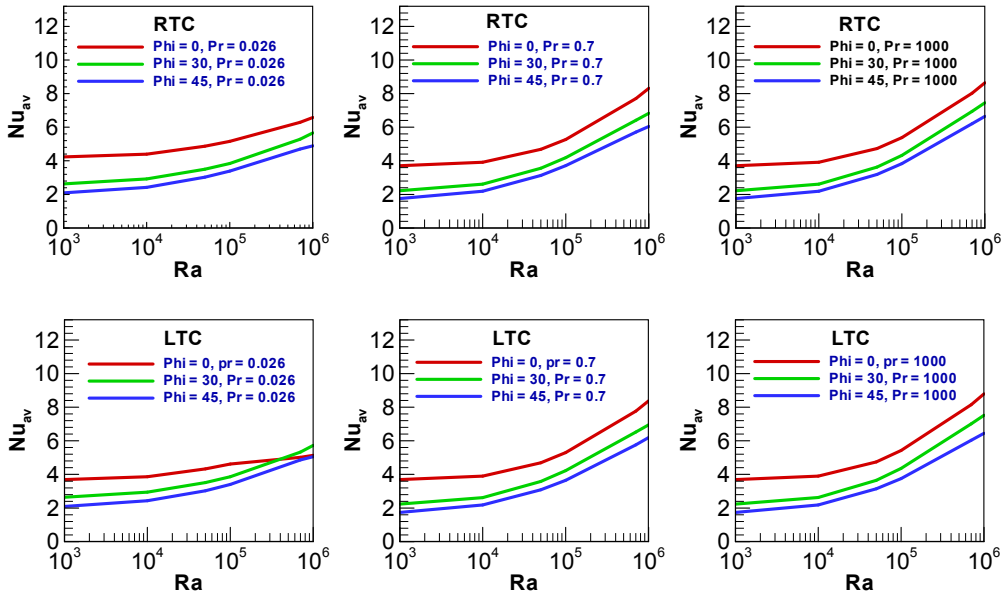

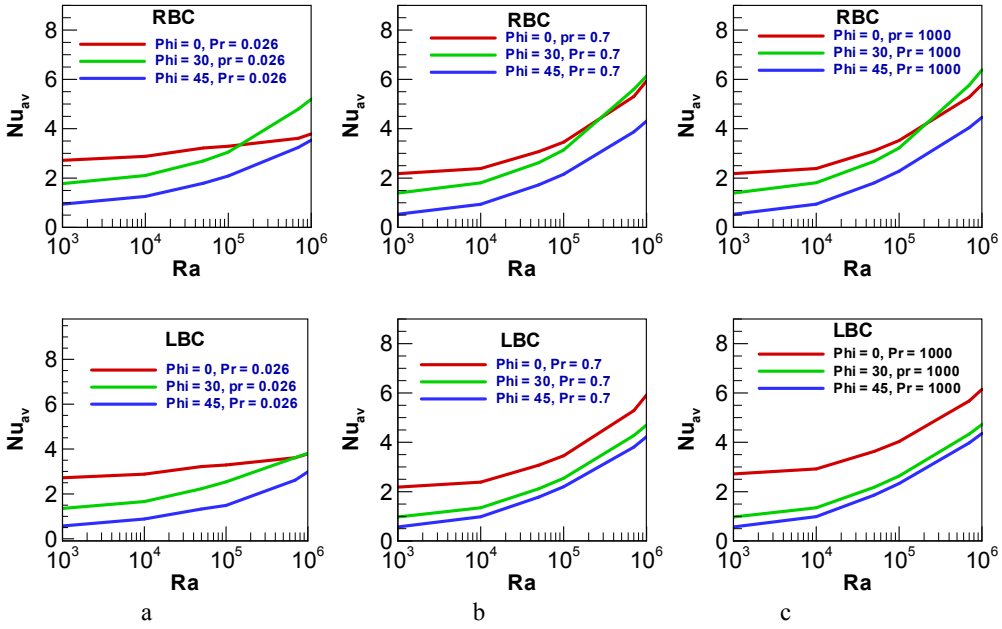

Fig. 17. Variations of Average Nusselt Number vs Rayleigh number for (a) Pr = 0.026, (b) Pr = 0.7, (c) Pr = 1000 and for various inclination of angles Φ = 0°, 30°, 45° in presence of non-uniform heating of LBC, RBC, LTC and RTC triangular block

8 Conclusion

In this exertion, a numerical analysis of natural convection flow in a trapezoidal cavity with a non-uniformly heated triangular block entrenched inside for different positions (LBC, RBC, LTC, and RTC) have been examined. A Galerkin weighted residual finite element method is used to solve nonlinear equations of conservation of mass, momentum, and energy equations for explanations of the nodal velocity component, temperature, and pressure with a wide range of parameters, such as, Prandtl numbers ,Pr (Pr = 0.026, 0.7, 1000) and Rayleigh numbers, Ra = 10^3 to 10^6. Streamlines, heatlines, pressure contours and isotherms over and above characteristics of heat transport organism has been assessed by the effect of non-uniformly hated triangular block. In the vision of the results presented, the major findings are summarised as follows:

- The outcomes lead to conclude that a little effect of different locations of the non-uniformly triangular block may be exposed on the fluid flow and the thermal fields for the range of Rayleigh numbers from 10^3 to 10^6 and Prandtl number from 0.026 to 1000 gradually.
- The heat generated by the inner different positions of the triangular block persuades notably both the shapes of stream functions (streamlines) and isotherm distributions and too it interrupts on the thickness of the thermal boundary layer.
- For the low Rayleigh number, the isotherms seem to be straight lines which are parallel to the side wall of the cavity, means that circulation of flow is weak. Due to non-uniformly heated triangular block, streamlines, isotherms and heatlines acquire highly curved non-uniform shape of a line when Rayleigh number increases.
- Streamlines, Isotherms, heatlines and pressure contours are highly condensed near the side walls and also beside the triangular block isotherms are compacted for ϕ = 30° and 45° for higher Ra = 10^6 and Pr = 0.026 to 1000. But the heatlines near the edges of the bottom wall exposes conductive heat transport for non-uniform heating of bottom wall which also occurs by the effect of triangular block. For non-uniformly heated triangular block, the heat is symmetrically distributed and the heatlines look likely tangential along the walls.

- For increasing value of Prandtl number the pressure contours are linear for Pr = 0.7 and 1000 with an inclinations of angles $\phi = 30^{\circ}$ and 45° for higher $Ra = 10^6$ and on account of enhancing various fluid circulations, the values of pressure contours increases at higher Prandtl number, Pr = 1000 and $Ra = 10^6$.
- Heat transfer rates for local Nusselt number are maximum near the edge of the side walls for all the positions (LBC, RBC, LTC, RTC) of non-uniformly heated triangular. The rate is minimum near to the west-south corner position of the wall for non-uniformly heated LBC triangular bock. The rate is also minimum near to the south-east corner position for non-uniformly heated RBC triangular bock and between the side (left) wall and near to centre of bottom wall due to non-uniformly heated LTC triangular bock. The rate is again minimum between near to centre of bottom wall and side (right) wall owing to non-uniformly heated RTC triangular bock irrespective of all tilt angles (ϕ) and also for Rayleigh number from 10^3 to 10^6 and Prandtl number from 0.026 to 1000 steadily. It means that heat transfer rate depends on different positions of non-uniformly heated triangular block, Rayleigh number and also Prandtl number.
- Heat transfer rate swells with swelling of Rayleigh number and thermal conductivity part.
- When the angle ϕ increases ($\phi = 0^{\circ}$, 30° and 45°) then average Nusselt number decreases but when Rayleigh number (Ra) increases from 10^3 to 10^6 gradually then average Nusselt number increases for all different positions of the non-uniformly heated triangular solid body surface.
- Different vortices such as primary vortices entering into the flow field and secondary vortex through the non-uniformly heated triangular block at the vicinity boundary wall and the bottom wall of the cavity are seen in the streamlines.

Acknowledgement

Authors would like to express their gratitude to the Department of Mathematics, Bangladesh University of Engineering and Technology (BUET), Dhaka-1000 and the Department of Arts and Sciences, Ahsanullah University of Science and Technology (AUST), Dhaka-1208 for providing computing facility during this work.

Competing Interests

Authors have declared that no competing interests exist.

References

[1] Swenson D, Hardeman B. The effects of thermal deformation on flow in a jointed geothermal reservoir. Int. J. Rock Mech. Min. Sci. 1997;34:e1-e20308.

[2] O'Mahoney D, Browne DJ. Use of experiment and an inverse method to study interface heat transfer during solidification in the investment casting process. Exp. Thermal Fluid Sci. 2000;22:111-122.

[3] Joudi KA, Hussein IA, Farhan AA. Computational model for a prism shaped storage solar collector with a right triangular cross- section. Energy Convers. Manage. 2004;45:391-409.

[4] Akterian SG, Fikiin KA. Numerical simulation of unsteady heat conduction in arbitrary shaped canned foods during sterilization processes. J. Food Eng. 1994;21:343-354.

[5] Park J, Kim SB, Kim HD, Choi SM. Natural convection heat transfer with crust formation in the molten metal pool. Nucl. Technol. 1999;127:66-80.

[6] Mishra B, Olson DL. Molten salt applications in materials processing. J. Phys. Chem. Solids. 2005;66:396-401.

[7] Basak T, Roy S, Singh A, Balakrishnan AR. Natural convection flows in porous trapezoidal enclosures with various inclination angles. International Journal of Heat and Mass Transfer. 2009(a);52(19-20):4612–4623.

[8] Basak T, Roy S, Singh A, Pop I. Finite element simulation of natural convection flow in a trapezoidal enclosure filled with porous medium due to uniform and non-uniform heating. International Journal of Heat and Mass Transfer. 2009;52(1-2):70-78.

[9] Basak T, Ramakrishna D, Roy S, Matta A, Pop I. A comprehensive heatline based approach for natural convection flows in trapezoidal enclosures: Effect of various walls heating. International Journal of Thermal Sciences. 2011;50(8):1385-1404.

[10] Basak T, Roy S, Matta A, Pop I. Analysis of heatlines for natural convection within porous trapezoidal enclosures: Effect of uniform and non-uniform heating of bottom wall. International Journal of Heat and Mass Transfer. 2010;53:5947–5961.

[11] Khozeymehnezhad H, Mirbozorgi SA. Comparison of natural convection around a circular cylinder with a square cylinder inside a square enclosure. Journal of Mechanical Engineering and Automation. 2012;2(6):176-183.

[12] Ramakrishna D, Basak T, Roy S, Momoniat E. Analysis of thermal efficiency via analysis of heat flow and entropy generation during natural convection within porous trapezoidal cavities. International Journal of Heat and Mass Transfer. 2014;77:98–113.

[13] Basak T, Roy S, Pop I. Heat flow analysis for natural convection within trapezoidal enclosures based on heatline concept. Int.J. Heat Mass Transfer. 2009;52:2471-2483.

[14] Hossain MS, Alim MA. MHD free convection within trapezoidal cavity with uniformly heated bottom wall. Annals of Pure and Applied Mathematics. 2013;3(1):41-55.

[15] Hossain MS, Alim MA. MHD free convection within trapezoidal cavity with non-uniformly heated bottom wall. International Journal of Heat and Mass Transfer. 2014;69:327–336.

[16] Aparna K, Seetharamu KN. Investigations on the effect of non-uniform temperature on fluid flowand heat transfer in a trapezoidal cavity filled with porous media. International Journal of Heat and Mass Transfer. 2017;108:63–78.

[17] Alsabery AI, Chamkha AJ, Hussain SH, Saleh H, Hashim I. Heatline visualization of natural convection in a trapezoidal cavitypartly filled with nanofluid porous layer and partly with non-Newtonianfluid layer. Advanced Powder Technology. 2015;26:1230–1244.

[18] Uddin H, Saha S. Study of natural convection flows in a tiltedtrapezoidal enclosure with isoflux heating from below. Suranaree J. Sci. Technol. 2008;15(4):293-306.

[19] Mebarek-oudina F, Bessaïh R. Numerical modeling of MHD stability in a cylindrical configuration. Journal of the Franklin Institute. 2014;351(2):667–681.

[20] Mebarek-oudina F, Bessaïh R. Oscillatory magnetohydrodynamic natural convection of liquid metal between vertical coaxial cylinders. J. of Applied Fluid Mechanics. 2016;9(4):1655-1665.

[21] Mebarek-oudina F. Numerical modeling of the hydrodynamic stability in vertical annulus with heat source of different lengths. Engineering Science and Technology. 2017;20:1324-1333.

[22] Mebarek-oudina F, Bessaïh R. Oscillatory mixed convection flow in a cylindrical container with rotating disk under axial magnetic field and various electric conductivity walls. I. Review of Physics. 2010;4(1):45-51.

[23] Mebarek-oudina F, Bessaïh R. Magnetohydrodynamic stability of natural convection flows in czochralski crystal growth. World Journal of Engineering. 2007;4(4):15–22.

[24] Reddy JN. An introduction to the finite element method. McGraw-Hill, New York; 1985.

[25] Bathe KJ. Finite element procedures. Prentice-Hall, New Jersey; 1996.

[26] Zienkiewicz OC, Taylor RL. The finite element method. Fourth Ed., McGraw-Hill; 1991.

© 2018 Hossain et al.; This is an Open Access article distributed under the terms of the Creative Commons Attribution License (http://creativecommons.org/licenses/by/4.0), which permits unrestricted use, distribution, and reproduction in any medium, provided the original work is properly cited.

Peer-review history:
The peer review history for this paper can be accessed here (Please copy paste the total link in your browser address bar)
http://www.sciencedomain.org/review-history/26101